Editors' Suggestion

Theory of reflectionless scattering modes

William R. Sweeney , 1,* Chia Wei Hsu , 2,3 and A. Douglas Stone , 1 Department of Physics, Yale University, New Haven, Connecticut 06520, USA

2 Department of Applied Physics, Yale University, New Haven, Connecticut 06520, USA

3 Ming Hsieh Department of Electrical and Computer Engineering, University of Southern California, Los Angeles, California 90089, USA

4 Yale Quantum Institute, Yale University, New Haven, Connecticut 06520, USA

(Received 9 September 2019; accepted 9 November 2020; published 7 December 2020)

We develop the theory of a special type of scattering state in which a set of asymptotic channels is chosen as inputs, and the complementary set is chosen as outputs, and there is zero reflection back into the input channels at specific frequencies. These states define perfectly impedance-matched input wavefronts for arbitrary finite scattering structures in any dimension. We find that an infinite number of such solutions exist at discrete frequencies in the complex ω (or energy) plane for any choice of the input-output sets under general conditions. Our results apply to linear electromagnetic and acoustic wave scattering and also, in many cases, to quantum scattering. We refer to such states as reflection-zeros (R-zeros) when they occur off the real-frequency axis and as reflectionless scattering modes (RSMs) when they occur or are tuned to the real-frequency axis and exist as steady-state harmonic solutions. The specific monochromatic input wavefront necessary is given by the eigenvector of a filtered scattering matrix with eigenvalue zero. RSMs may be realized either by tuning parameters of the scatterer which preserve flux conservation (index tuning) or by adding gain or absorption (gain-loss tuning), which do not. We show that in general only a single continuous system parameter needs to be tuned to create an RSM from an R-zero for a given choice of input-output channels for both guided wave and free-space excitation. In addition, a coupled-mode analysis shows that RSMs are the result of a generalized type of critical coupling. A symmetry analysis of R-zeros and RSMs implies that RSMs of flux-conserving cavities or structures are bidirectional: the input and output channels can be interchanged and the resulting state will also be an RSM at the same frequency. RSMs of cavities with gain and/or absorption are generically unidirectional, and do not satisfy this interchange symmetry. Non-flux-conserving systems with $\mathcal{P}T$ symmetry have unidirectional R-zeros in complex-conjugate pairs, implying that for small enough \mathcal{T} breaking their reflectionless states arise at real frequency, without the need of any parameter tuning. This explains the widely observed existence of unidirectional unit transmission resonances in one-dimensional $\mathcal{P}T$ systems, and their disappearance as a result of spontaneous $\mathcal{P}T$ -symmetry breaking. An alternative type of exceptional point is shown to occur at this transition, leading to an observable change in the reflection and/or transmission line shape. Numerical examples of RSMs are given for one-dimensional cavities with and without gain or loss, a one-dimensional PT cavity, a two-dimensional multiwaveguide junction, and a two-dimensional deformed dielectric cavity in free space. We outline and implement a general technique for solving such problems, which shows promise for designing photonic structures which are perfectly impedance matched for specific inputs, or can perfectly convert inputs from one set of modes to a complementary set.

DOI: 10.1103/PhysRevA.102.063511

I. INTRODUCTION

A. Resonant impedance matching of waves

Resonant scattering of waves is a fundamental process in classical and quantum physics. At certain input frequencies or energies, incident waves impinging on an object or inhomogeneous region ("the scatterer") can excite normal modes of oscillation of the scatterer, leading to strong scattering and relatively long interaction times. The normal modes of any such open system are resonances, alternatively called quasinormal modes or Gamow states, which correspond to purely outgoing solutions of the wave equation with complex frequencies,

 $\omega = \omega_r - i\gamma$, where $\gamma = 1/2\tau > 0$, τ is the dwell time or intensity decay rate, and $Q = \omega_r \tau$ is the quality factor of the resonance [1–4]. In general, the resonances are not physically realizable steady states due to their exponential growth at infinity, but they determine the scattering behavior under steady-state (real-frequency) harmonic excitation. However, in electromagnetic scattering with gain, the resonances *can* be realized physically and correspond to the onset of laser emission [5–7]. This threshold lasing state is a solution of the linear Maxwell wave equation for a scattering geometry, but with no incident wave; it can only be realized at discrete frequencies and with the appropriate amount of gain to balance exactly scattering and absorption loss.

While every finite structure will support resonances when excited at wavelengths shorter than the size of the

^{*}william.sweeney@yale.edu

structure, there is, to our knowledge, no general theory of the conditions under which those resonances are accompanied by reflectionless or perfectly impedance-matched input states under steady-state harmonic excitation. The effectively one-dimensional (1D) examples found in textbooks and implemented in optical and electronic technology suggest that parity symmetric lossless scattering structures (e.g., a perfect Fabry-Pérot resonator, or balanced double barrier systems in quantum mechanics) do have reflectionless input states at a frequency equal to or close to the real part of each resonance frequency, and that, if parity is broken, such states do not exist. In all branches of wave physics it is common to excite more complex structures near their resonances in order to strongly couple waves into or through the structure, and it is usually highly desirable that this excitation not reflect energy back to the source. While there has certainly been extensive work on reducing reflection from many specific structures, to our knowledge there is little prior theoretical or experimental work on the necessary and sufficient conditions for the existence of impedance-matched input states in any geometry that is not effectively one-dimensional. This question, and the question of how to construct such states when they exist, are the focus of the current paper.

Some time ago the necessary and sufficient conditions for the existence of a certain type of reflectionless state in structures of arbitrary complexity were established in work by one of the current authors (and coworkers). These are states which correspond to the time reverse of the resonances, satisfying the boundary conditions that there are only incoming waves at a sufficient distance from the structure. For lossless structures (or Hermitian Hamiltonians in quantum mechanics) these states were already well known for many decades, since they occur at the conjugate of the complex resonance frequencies (and are not physically realizable for the same reason), but in 2010 it was pointed out that, just as gain can be added to a cavity to create a laser at threshold, a lossy material could be added to the same cavity such that the purely incoming solution (by time-reversal symmetry) was equivalent to a perfectly impedance-matched state at the same (real) frequency, a phenomenon now known as coherent perfect absorption (CPA) [8–10]. This time-reversed solution of lasing at threshold is simply the complex conjugate of the outgoing lasing mode. Importantly, the absorption is perfect only for that structure-specific wavefront, at that specific frequency. Thus to achieve CPA for a complex structure one has to synthesize the appropriate complex incoming wavefront, and adjust the loss in the cavity to a precise value (the same magnitude and spatial distribution as the gain of the corresponding laser). The theory of CPA proves the existence of resonant perfectly impedance-matched solutions for arbitrarily complex structures in any dimension, when the input wavefront, frequency, and loss are appropriately tuned.

However, CPA is just one very special type of reflectionless input state, one for which all accessible input channels are filled and no energy is radiated outwards. In this case, all of the input energy is trapped in the scatterer or cavity and absorbed in the lossy medium (which we assume is able to dissipate the power generated without significant nonlinear effects). An interesting recent work has studied CPA in a disordered microwave cavity with multiple antenna inputs [11]. The setup

is interesting because the basic source of "absorption" is an internal antenna and the input channels are the multiple external antennas. In some parameter ranges where full absorption is measured, almost all of the energy is detected at the internal antenna and is not absorbed irreversibly by the structure, while in other ranges both the internal antenna and the cavity absorption contribute. While these experiments are quite interesting, for reasons which should become clear below, we regard them as examples of the more general reflectionless states defined here, and not true CPA, as outgoing radiation through the internal antenna is not irreversible energy dissipation. Of course, more generally wave physicists are interested in reflectionless states of this kind, in which a subset of the scattering channels is used as inputs, which then are either completely transmitted through the structure to some designated output channels, or possibly are partially absorbed (or even amplified) in the structure along the way, but nonetheless radiate energy into the output channels. This general notion of reflectionless states is addressed in the current paper, which includes CPA as a special case.

Another relatively recent example of perfectly impedancematched states which has been extensively studied is the perfect transmission resonances of structures with symmetric absorption and gain distributions (i.e., parity-time symmetric, PT). PT structures in optics have gotten much recent attention [12–20]. Specifically, 1D open PT structures exhibit reflectionless states [21–35], which are unidirectional. Since such structures are not lossless, in general photon flux is not conserved, so it is possible and in fact generically true that a structure which supports a reflectionless state traveling from left to right at a given frequency will not be reflectionless for a wave incident from the right at the same frequency. Much of this work is summarized in a recent review [36]. While these unidirectional reflectionless resonances are present in all PT structures, they apparently disappear at sufficiently high frequency for a fixed value of gain-loss [22–25,37]. The unidirectional reflectionless states do occur in conjunction with standard scattering resonances, but in the PT case they are typically substantially shifted in frequency from the real part of the resonance frequency (see Fig. 3 below). One-way reflectionless states have also been studied in non-flux-conserving systems that do not possess PT symmetry [37–43], including those supporting constantintensity waves [44,45].

In the current paper we will show how these previously known cases-reflectionless states of simple paritysymmetric structures, perfectly absorbed CPA states, and unidirectional $\mathcal{P}T$ -symmetric reflectionless states—fit into a more general theory of reflectionless states, which is formulated in the following manner. In any linear scattering system of finite spatial extent there will be a finite number of asymptotic scattering channels that are relevant, and we can choose a subset of the asymptotic channels as the input channels. Based on this choice, we define a set of states by the condition that they are scattering solutions for which no energy is reflected back into the chosen channels at the input frequency, assuming an appropriate wavefront is chosen for the input channels. We will show that, generically, a countably infinite set of such reflectionless scattering states exists at discrete complex frequencies (similar to resonances); we

will refer to these frequencies and corresponding wavefronts as *reflection zeros* or *R*-zeros. Through parameter tuning or by imposing symmetry, an *R*-zero can be moved to a real frequency to become a steady-state solution that we refer to as a *reflectionless scattering mode* (RSM). In this way the RSM concept is similar to CPA, and shares the attribute that such RSMs exist in arbitrarily complex systems for the appropriate input wavefront, if a single parameter is tuned.

But the RSM is more general, because it encompasses all possible exciting wavefronts and does not require that all input channels be used. Hence it corresponds to the more typical situation in which impedance matching is desired in order to avoid reflection and transmit all or most of the incident energy through the structure. Moreover the R-zero-RSM formulation applies to systems that do not naturally divide into left and right asymptotic regions. Any subset of the asymptotic channels may be chosen as inputs, with the complementary set being the outputs, even when the input and output channels spatially overlap. We will show how, for any choice of input channels, R-zeros and RSMs can be found computationally for any specific cavity or structure of interest, and will give nontrivial examples of RSMs in multichannel and free-space structures, which are obtained in our method without searching a large space and using iterative optimization. The computational methods are of similar difficulty to calculating resonances of complex structures, and in many cases the perfectly matched layer (PML) or complex scaling method can be used [46,47]. For other important cases (such as free-space RSMs) the PML method cannot be used, but a slightly more complicated boundary-matching technique can be implemented. No particular symmetry of the structure is required in order for it to have an RSM at a given frequency, however we will analyze in detail the effect of discrete symmetries on R-zeros and RSMs before giving more general examples.

A recent published work [48] is closely related to the present one. The authors introduce the concept of reflectionless modes in the context of waveguides, but only define reflectionless modes in terms of left to right (or right to left) transmission and not in terms of arbitrary partitions of all asymptotic modes, as we do here. They specifically emphasize and demonstrate that the R-zero spectrum is distinct from the usual resonance spectrum even when the R-zeros are complex, and introduce in this context a multimode reflection matrix, which is a special case of our generalized reflection matrix defined in Sec. II A below. However the examples shown do not require finding a nontrivial input state adapted to the scatterer, as in the more general cases we present below, and there is no discussion of this crucial point. While their work has significant overlap with the work presented here, there are substantial differences. The authors define R-zeros only for waveguides and, as noted, only for the case of choosing all of the input modes on one side and all of the output modes on the other, whereas in our approach any mode on either side can be chosen as an input and output mode in defining the impedance-matching problem. With these restrictions, their notion of reflectionless modes is directly tied to the PML method, which can only be applied when input and output modes are spatially separated. Important cases where the PML method cannot be used to find RSMs are finite-sized scatterers or antennas in free space (see Fig. 6 below), or planar scatterers illuminated with a finite numerical aperture (where the input channels consist of a subset of incident angles), or multimode waveguides with input and output channels occurring in the same waveguide, as for certain types of mode converters. The tuning of *R*-zeros to the real axis, which will be necessary in almost all nontrivial cases, is not discussed at all in Ref. [48] and no connection is made to the longstanding notion of critical coupling to avoid reflection. Finally, there is no discussion of tuning to an RSM exceptional point (EP), and of the physics at such a point, which differs from almost all previous work on EPs and sheds light on the PTsymmetry-breaking transition as we discuss below. The notion of parameter tuning of R-zeros to achieved generalized form of critical coupling is central to this paper. We will provide two methods to find R-zeros in these more general cases, involving either a filtered scattering matrix or the underlying wave operator, and derive an explicit connection between the two methods that also highlights the role of bound states in the continuum [49]. In the wave-operator approach, incoming and outgoing boundary conditions for arbitrary choices of channels can be implemented through the boundary-matching methods [50] (see Sec. IIF2).

Critical coupling is a longstanding idea in optical and electromagnetic wave physics [51–53]: when coupling into a cavity through a single input channel at the frequency of a well-isolated cavity resonance, zero reflection occurs when the rate of input coupling equals the rate of loss in the cavity. The literature is somewhat unclear as to whether it makes a difference if the loss is radiative or dissipative or a combination of the two. Many practical photonic devices use critical coupling, and there are devices which operate in either limit. The RSM concept introduced here does reduce to critical coupling for the case of a single input channel coupled to an isolated resonance and makes it clear that for zero reflection it does not matter if the loss is radiative or dissipative. However the RSM theory shows how to achieve zero reflection with multiple input channels and when resonances overlap (both aspects are illustrated in Fig. 5 below). It also adds to the critical coupling condition the additional requirement that one needs to send in a specific coherent wavefront to achieve zero reflection, which is not necessary for the case of a single input channel. Hence the RSM theory can be used to achieve impedance matching in more complex structures and geometries, as well as to achieve perfect mode conversion, and we believe it opens up a promising approach to design of photonic structures. Moreover, the RSM concept applies to a wide variety of wave scattering systems, for example sound waves, waves of cold atoms or condensates, and other quantum systems with short-range interactions. Unlike lasing and CPA, which are nonunitary by definition (i.e., do not conserve energy flux), steady-state RSMs can be flux conserving and do not require the availability of absorption or gain as a design resource. We will discuss engineering of passive RSMs (without loss or gain) below.

B. Scattering matrix

To make the RSM concept more precise we must now introduce the starting point of the theory, the scattering matrix

(S matrix) of an open wave system. The system generally consists of an inhomogeneous scattering region, outside of which are asymptotic regions that extend to infinity. To support resonance effects the scattering region needs to be larger than the wavelength of the input waves within the scattering medium. The asymptotic regions are assumed to be time-reversal invariant and to have some form of translational invariance, e.g., vacuum or uniform dielectric, or a finite set of waveguides, or an infinite periodic photonic crystal. We also focus on media in which the scattering forces are short-range, so that the complications associated with long-range Coulomb or other forces are absent. This limits the application of the theory for certain problems in quantum scattering or in plasma scattering but this simplification holds for the scattering of electromagnetic and sound waves in almost all cases; for the remainder of this paper we will develop the theory in terms of classical Maxwell

A linear and static photonic structure is described by its dielectric function $\varepsilon(\mathbf{r},\omega)$, which can be complex-valued, in which case its imaginary part describes absorption and/or gain. The assumed linearity allows the theory to concentrate on scattering at a single real frequency, ω ; time-dependent scattering can be studied by superposing solutions. The translational symmetry of the asymptotic regions allows one to define 2N power-orthogonal propagating "channel states" at each ω . Based on the direction of their fluxes, the 2N channels can be unambiguously grouped into N incoming and N outgoing states, which are related by time reversal. Familiar examples of channels include the guided transverse modes of a waveguide and orbital angular momentum waves in free space, with one channel per polarization. In the waveguides, the finite number and width of the waveguides lead to a finite N for a given ω , whereas for the case of a finite scatterer or cavity in free space the number of propagating angular momentum channels is countably infinite. However, a finite scatterer of linear scale R, with no long-range potential outside, will interact with only a finite number of angular momentum states, such that $l_{\rm max} \sim \sqrt{\bar{\epsilon}} R\omega/c$, where $\bar{\epsilon}$ is the spatially averaged dielectric function in the scattering region, and c is the speed of light. Hence for each ω we can reasonably truncate the infinite-dimensional channel space to a finite, N-dimensional subspace of relevant channels.

A general scattering process then consists of incident light, propagating along the N incoming channels, interacting with the scatterer and then propagating out to infinity along the N outgoing channels, as illustrated in Fig. 1(a). The partial scattering of a single incoming channel into the outgoing channel which is its time reverse defines a reflection coefficient, and scattering into each other channel defines the transmission coefficients. In the channel basis, the wavefronts of the incoming and outgoing fields are given by length-N column vectors α and β , normalized such that $\alpha^{\dagger}\alpha$ and $\beta^{\dagger}\beta$ are proportional to the total incoming and total outgoing energy flux, respectively. The N-by-N scattering matrix $S(\omega)$, which relates α and β at frequency ω , is defined by

$$\boldsymbol{\beta} = \mathbf{S}(\omega)\boldsymbol{\alpha}.\tag{1}$$

In a partitioned (left-right) geometry the elements of the S matrix are all of the transmission and reflection amplitudes between the channels; in a general geometry they are just

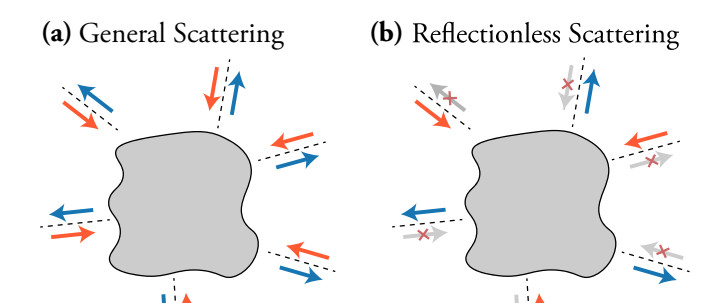


FIG. 1. (Color) Schematic depicting a general scattering process (a) and reflectionless process (b). A finite scatterer or cavity interacts with a finite set of asymptotic incoming and outgoing channels, indicated by the red inward-pointing and blue outward-pointing arrows, respectively, related by time reversal. These channels may be localized in space (e.g., waveguide channels) or in momentum space (e.g., angular momentum channels). (a) In the general case without symmetry, all incoming channels will scatter into all outgoing channels. (b) There exist reflectionless states, for which there is no reflection back into a chosen set of incoming channels (the inputs), which in general occur at discrete complex frequencies and do not correspond to a steady-state harmonic solution of the wave equation. However, with variation of the cavity parameters, a solution can be tuned to have a real frequency, giving rise to a steady-state reflectionless scattering process for a specific coherent input state, referred to as a reflectionless scattering mode (RSM).

interchannel scattering amplitudes. Below we will define a generalized reflection matrix from the S matrix in an arbitrary geometry. In reciprocal systems, the S matrix is symmetric, $S = S^T$ [54]. If the scatterer is lossless (i.e., ε is real everywhere), then any incoming state leads to a nonzero flux-conserving output, and the S matrix is unitary.

The S matrix, being well defined at all real frequencies (absent self-oscillating solutions, i.e., lasing), can be extended to complex frequencies via analytic continuation.

II. GENERAL THEORY OF R-ZEROS AND RSMs

We will now define *R*-zeros and RSMs for a general geometry, prove the existence of solutions in the complex-frequency plane, and analyze the properties of *R*-zeros and RSMs based on the existence of different symmetries of the scattering system.

A. R-zeros and RSMs

R-zeros are specific solutions of the scattering problem, typically at a complex frequency, for which there is no back-reflection into a given set of channels. A RSM occurs when an R-zero is tuned to a real frequency, and is therefore a specially constrained steady-state solution of the more general R-zero problem. To define an R-zero problem, we specify $N_{\rm in}$ of the incoming channels to be "input channels" which carry incident flux but no outgoing flux, and are thus reflectionless, with $0 < N_{\rm in} < N$. The complementary set of $N_{\rm out} = N - N_{\rm in}$ outgoing channels (the "output channels") carries any outbound flux. This is illustrated in Fig. 1(b).

Let $\alpha_{\rm in}$ denote the $N_{\rm in}$ -component vector containing the input amplitudes of such a reflectionless incident field, and $\mathbf{R}_{\rm in}(\omega)$ denote the square $N_{\rm in}$ -by- $N_{\rm in}$ "generalized reflection matrix," which is the submatrix of the analytically continued $\mathbf{S}(\omega)$ defined by the specified input channels, i.e., $(R_{\rm in})_{i,j} = S_{n_i,n_j}$, where $i,j=1,2,...,N_{\rm in}$ and $\{n_i\}$ is the set of $N_{\rm in}$ channels. At the complex frequency $\omega_{\rm RZ}$ of an R-zero, the absence of reflection can be expressed as

$$\mathbf{R}_{\rm in}(\omega_{\rm RZ})\boldsymbol{\alpha}_{\rm in} = \mathbf{0},\tag{2}$$

which is the formal definition of an R-zero. In other words, the R-zero frequencies are those at which $\mathbf{R}_{\rm in}(\omega)$ has a zero eigenvalue, the corresponding eigenvector $\alpha_{\rm in}$ being the reflectionless incident wavefront. More generally, Eq. (2) defines a nonlinear eigenproblem where $\omega_{\rm RZ}$ is the eigenvalue, and methods for solving general nonlinear eigenproblems [55–59] may be used to solve it.

Equation (2) can also be solved by finding the roots of the complex scalar function det $\mathbf{R}_{in}(\omega)$:

$$\det \mathbf{R}_{\rm in}(\omega_{\rm RZ}) = 0. \tag{3}$$

Since the generalized reflection matrix can be computed for any open scattering system using standard methods, Eqs. (2) and (3) provide universal recipes for solving the R-zero problem, for each of the $2^N - 2$ choices of reflectionless input channels.

We will show in Eq. (16) in Sec. II C that, generically, near each zero to leading order det $\mathbf{R}_{in}(\omega) \propto (\omega - \omega_{RZ})$, so that the phase angle $arg(det \mathbf{R}_{in})$ winds by 2π along a counterclockwise loop around each ω_{RZ} in the complex-frequency plane. One may regard each R-zero as a topological defect in the complex-frequency plane with a topological charge of +1 [60]. As such, R-zeros are robust: when the optical structure $\varepsilon(\mathbf{r})$ is perturbed, ω_{RZ} moves in the complex-frequency plane but cannot suddenly disappear, similar to topological defects in other systems [61,62]. For an R-zero to disappear, it must annihilate with another topological defect of $\det \mathbf{R}_{in}$ with charge -1. We will show in Sec. II C that such a charge annihilation leads to either a bound state in the continuum or a single-side resonance, where $\det \mathbf{R}_{in}$ is neither zero nor infinity. When parameters of the system are tuned such that n > 1 R-zeros meet at the same frequency, they superpose and form a topological defect with charge +n where det $\mathbf{R}_{\mathrm{in}} \propto$ $(\omega - \omega_{RZ})^n$; we will show later that these are EPs of a wave operator and provide an explicit example in Figs. 3(b)-3(e).

Even though the case of $N_{\rm in}=N$ leads to a well-defined $\mathbf{R}_{\rm in}=\mathbf{S}$, we will exclude it from the ensuing discussion since the corresponding $\omega_{\rm RZ}$ is already understood as a zero of the S matrix [8], and for flux-conserving systems is constrained to the upper half of the complex-frequency plane, and unlike other R-zeros cannot be tuned to the real axis (CPA) without adding loss. The case $N_{\rm in}=0$, corresponding to resonance, is also excluded, as here $\mathbf{R}_{\rm in}$ and the associated R-zeros are not defined.

The simultaneous absence of reflection in all input channels for the R-zero incident wavefront is due to interference: the reflection amplitude of each input channel i destructively interferes with the interchannel scattering from all the other input channels, $(R_{\rm in})_{ii}\alpha_i + \sum_{j\neq i}(R_{\rm in})_{ij}\alpha_j = 0$, which is precisely Eq. (2). The scattering ("transmission") into the output

channels is not obtained from solving this equation alone, and must be determined by solving the full scattering problem at ω_{RZ} .

While Eq. (2) or Eq. (3) already provides a concrete recipe for finding R-zeros, we will further analyze $\det \mathbf{R}_{in}(\omega)$ to shed light on the existence of R-zeros in the complex-frequency plane and to reveal their relation to the wave operator and to resonances in the next two sections.

B. Wave-operator representation of the S matrix

In this section, we introduce a wave-operator representation of $\mathbf{S}(\omega)$ and det $\mathbf{S}(\omega)$, which we will adapt in the next section to analyze $\mathbf{R}_{\text{in}}(\omega)$ and det $\mathbf{R}_{\text{in}}(\omega)$. Throughout this paper we focus on the Fourier representations of the wave equation appropriate for the study of harmonic scattering solutions and will use the term *wave operator* to refer to the relevant differential operators in the frequency domain as defined below. This differs from how the term is typically used in the mathematical theory of wave scattering, as presented in Ref. [63].

Consider a wave operator $\hat{A}(\omega)$ acting on state $|\omega\rangle$, which satisfies $\hat{A}(\omega) |\omega\rangle = 0$.

For electromagnetic scattering, $\langle \mathbf{r} | \omega \rangle$ is the magnetic field, $\mathbf{H}(\mathbf{r})$, under harmonic excitation at ω , and the Maxwell operator at frequency ω is given by

$$\langle \mathbf{r}' | \hat{A}(\omega) | \mathbf{r} \rangle = \delta(\mathbf{r} - \mathbf{r}') \left\{ \left(\frac{\omega}{c} \right)^2 - \nabla \times \left(\frac{1}{\varepsilon(\mathbf{r})} \nabla \times \right) \right\}. \quad (4)$$

Divide the system into two regions: the finite, inhomogeneous scattering region Ω in the interior, and the exterior asymptotic region $\bar{\Omega}$ that extends to infinity, which possesses a translational invariance broken only by the boundary, $\partial \Omega$, between Ω and $\bar{\Omega}$. We separate the operator $\hat{A}(\omega)$ into three pieces:

$$\hat{A}(\omega) = [\hat{A}_0(\omega) \oplus \hat{A}_c(\omega)] + \hat{V}(\omega). \tag{5}$$

 $\hat{A}_0(\omega)$ acts in the interior region Ω , $\hat{A}_c(\omega)$ acts in the exterior region $\bar{\Omega}$, and both are identical to $\hat{A}(\omega)$ in their respective domains. The coupling term $\hat{V}(\omega)$ between the two regions is defined via $\hat{V}(\omega) \equiv \hat{A}(\omega) - [\hat{A}_0(\omega) \oplus \hat{A}_c(\omega)]$.

The auxiliary, closed-cavity wave operator $\hat{A}_0(\omega)$ on Ω , subject to Neumann boundary conditions, admits a discrete spectrum of the form $\hat{A}_0(\omega_\mu) | \mu \rangle = 0$ with eigenvalues $\{\omega_\mu\}$. We use this nonstandard definition of the eigenvalue to be consistent with the formulation of nonlinear eigenvalue problems [55–59], where the operator $A(\omega)$ depends nonlinearly on ω , a case which will be relevant shortly in the computation of resonances and R-zeros. We explicitly do not assume $\hat{A}_0(\omega)$ to be Hermitian, as one major focus of this paper is to use absorption or gain to tune the R-zeros frequencies to become real, creating an RSM. The matrix $\mathbf{A}_0(\omega)$ is naturally defined by its matrix elements:

$$A_0(\omega)_{\mu\nu} = \langle \mu | \hat{A}_0(\omega) | \nu \rangle. \tag{6}$$

The auxiliary asymptotic wave operator $\hat{A}_c(\omega)$ on $\bar{\Omega}$, subject to a Neumann boundary condition at its interface with the scatterer, has a continuum of solutions. It generates the propagating channel modes via $\hat{A}_c(\omega)|\omega,n\rangle=0$ (n here is an integer or set of integers which uniquely specifies the asymptotic channels for each real frequency, ω). By construction, the

only nonvanishing matrix elements of \hat{V} are those between closed and continuum states, so that the matrix $\mathbf{W}(\omega)$, not necessarily square, is given by

$$W(\omega)_{\mu n} = \langle \mu | \hat{V}(\omega) | n, \omega \rangle, \tag{7}$$

and contains all the information in $\hat{V}(\omega)$.

A general relation [64–67] between the matrices S, A_0 , and W, originally developed in the study of nuclear reactions as the continuum-shell model or shell-model approach [64,68–75], is

$$\mathbf{S}(\omega) = \mathbf{I}_N - 2\pi i \mathbf{W}_p^{\dagger}(\omega) \mathbf{G}_{\text{eff}}(\omega) \mathbf{W}_p(\omega), \tag{8}$$

where \mathbf{I}_N is the *N*-by-*N* identity, and the effective Green's function $\mathbf{G}_{\text{eff}}(\omega)$ is the inverse of the effective wave operator $\mathbf{A}_{\text{eff}}(\omega)$:

$$\mathbf{G}_{\text{eff}} \equiv \mathbf{A}_{\text{eff}}^{-1}, \quad \mathbf{A}_{\text{eff}} \equiv \mathbf{A}_{0}' - \mathbf{\Sigma}^{R},$$

$$\mathbf{\Sigma}^{R} \equiv \mathbf{\Delta} - i\mathbf{\Gamma}, \quad \mathbf{\Gamma} \equiv \pi \mathbf{W}_{p} \mathbf{W}_{p}^{\dagger},$$

$$\mathbf{\Delta}(\omega) \equiv \text{p.v.} \int d\omega' \frac{\mathbf{W}_{p}(\omega') \mathbf{W}_{p}^{\dagger}(\omega')}{\omega' - \omega}.$$
(9)

For conciseness we have suppressed and will continue to suppress the dependence on ω , except when needed for clarity. The matrix \mathbf{W}_p is the full coupling matrix \mathbf{W} restricted to the N propagating channels, while \mathbf{A}_0' is the closed-cavity wave operator \mathbf{A}_0 plus a Hermitian modification that includes the effect of evanescent channel states. The operator $\mathbf{\Sigma}^R$ is the self-energy, and acts only on the boundary $\partial \Omega$; $\mathbf{\Delta}$ and $-i\mathbf{\Gamma}$ are its Hermitian and anti-Hermitian components.

The resonances of the system are the eigenmodes of the non-Hermitian, nonlinear eigenvalue problem $\hat{A}_{\rm eff}(\omega_p)|\omega_p\rangle=0$, with eigenvalues $\{\omega_p\}$ that are the complex-valued resonance frequencies, which generally form a countably infinite set. Note that the frequency dependence of the self-energy makes the eigenproblem nonlinear. Since Γ is positive semidefinite, the self-energy due to openness generally contributes a negative imaginary part to the resonance frequencies, pushing the poles of $G_{\rm eff}(\omega)$ and $S(\omega)$ into the lower half of the complex-frequency plane, exactly capturing the effect of openness.

A series of manipulations applied to Eq. (8) yields a powerful identity for det $\mathbf{S}(\omega)$. Using the "push-through identity" of linear algebra [76], we move the interaction matrix \mathbf{W}_p across $\mathbf{G}_{\mathrm{eff}}$ to obtain $\mathbf{S} = (\mathbf{1} + i\mathbf{K})/(\mathbf{1} - i\mathbf{K})$, where the reactance matrix $\mathbf{K} \equiv -\pi \mathbf{W}_p^{\dagger} (\mathbf{A}_0' - \mathbf{\Delta})^{-1} \mathbf{W}_p$ [77,78]. Taking the determinant of both sides and dividing numerator and denominator by $\det(\mathbf{A}_0' - \mathbf{\Delta})$, we arrive at

$$\det \mathbf{S}(\omega) = \frac{\det \left(\mathbf{A}_0'(\omega) - \mathbf{\Delta}(\omega) - i\mathbf{\Gamma} \right)}{\det \left(\mathbf{A}_0'(\omega) - \mathbf{\Delta}(\omega) + i\mathbf{\Gamma} \right)}.$$
 (10)

Note that Eq. (10) is not a simple identity of linear algebra: the left-hand side is the standard determinant of an *N*-by-*N* square matrix, while the right-hand side is a ratio of functional determinants of differential operators on an infinite-dimensional Hilbert space. See Appendix A1 for more detail on the derivation of Eq. (10). A related expression was given in Refs. [79,80].

Equation (10) reveals that the analytically continued $\det \mathbf{S}(\omega)$ has zeros at a countably infinite set of complex

frequencies $\{\omega_z\}$, which are the eigenvalues of the nonlinear eigenproblem $[\hat{A}_0(\omega_z) - \hat{\Sigma}^A(\omega_z)]|\omega_z\rangle = 0$, where $\hat{\Sigma}^A = \hat{\Delta} + i\hat{\Gamma}$; we refer to them as the *zeros of the S matrix*. CPA arises when, by tuning the degree of absorption in the system, one member of this set reaches a real frequency and becomes a steady-state solution. As described in the introduction, the time reverse of CPA is threshold lasing (purely outgoing solutions at real frequency). We can now generalize that as follows: the time reverse of the state corresponding to a complex zero of the S matrix is a resonance. For a lossless scatterer, time-reversal symmetry implies that $\omega_z = \omega_p^*$, which is consistent with Eq. (10) since $(\hat{\Sigma}^A(\omega))^{\dagger} = \hat{\Sigma}^R(\omega^*)$ when $\varepsilon(\mathbf{r})$ is real.

While an eigenvalue of $\hat{A}_0(\omega) - \hat{\Sigma}^R(\omega)$ typically corresponds to a pole of det $\mathbf{S}(\omega)$ and an eigenvalue of $\hat{A}_0(\omega) - \hat{\Sigma}^A(\omega)$ to a zero of det $\mathbf{S}(\omega)$, there is one important exception. Equation (10) shows that if $\omega_p = \omega_z$ is the simultaneous eigenvalue of both, det $\mathbf{S}(\omega)$ may be neither zero nor infinite. Such an exception happens at a bound state in the continuum (BIC) [49], which contains neither incoming nor outgoing radiation and exists at a real frequency for passive structures. A BIC is invariant under time reversal, and does not affect $\mathbf{S}(\omega)$ since it is decoupled from far-field radiation. In the topological-defect picture, a BIC implies that a +1 charge (S-matrix zero) annihilates with an -1 charge (resonance) on the real axis.

C. Analytic properties of R-zeros and RSMs

We now adapt this formalism to treat R-zeros and RSMs, which can be analyzed in a similar fashion through the relation between the generalized reflection matrix \mathbf{R}_{in} and the S matrix. Let F be the set of N_{in} filled input channels, which fixes \bar{F} , the set of N_{out} filled output channels (the remaining incoming and outgoing channels will carry no flux). Because the channel ordering in \mathbf{S} is arbitrary, for convenience we permute \mathbf{S} such that the N_{in} input channels correspond to the upper-left block of \mathbf{S} , namely,

$$\mathbf{S}(\omega) = \begin{pmatrix} \mathbf{R}_{\text{in}}(\omega) & \mathbf{T}_{2}(\omega) \\ \mathbf{T}_{1}(\omega) & \mathbf{R}_{\text{out}}(\omega) \end{pmatrix}. \tag{11}$$

To extract \mathbf{R}_{in} from \mathbf{S} , let us define the filtering matrices \mathbf{F} and $\bar{\mathbf{F}}$, where $\mathbf{F}: \mathbb{C}^N \to \mathbb{C}^{N_{\text{in}}}$ reduces the dimension of the channel space from N to N_{in} , i.e., $F_{ij} = \delta_{c(i),j}$ where c(i) is the ith input channel, with $i \leq N_{\text{in}}$, $j \leq N$, and $\bar{\mathbf{F}}$ reduces from N to N_{out} . It follows that

$$\mathbf{F}\mathbf{F}^{\dagger} = \mathbf{I}_{N_{\text{in}}}, \quad \bar{\mathbf{F}}\bar{\mathbf{F}}^{\dagger} = \mathbf{I}_{N_{\text{out}}}, \quad \mathbf{F}^{\dagger}\mathbf{F} + \bar{\mathbf{F}}^{\dagger}\bar{\mathbf{F}} = \mathbf{I}_{N}.$$
 (12)

With these definitions we have

$$\mathbf{R}_{\rm in}(\omega) = \mathbf{F}\mathbf{S}(\omega)\mathbf{F}^{\dagger}.\tag{13}$$

Using Eqs. (8) and (13),

$$\mathbf{R}_{\text{in}} = \mathbf{I}_{N_{\text{in}}} - 2\pi i \mathbf{W}_{F}^{\dagger} \mathbf{G}_{\text{eff}} \mathbf{W}_{F},$$

$$\mathbf{W}_{F} \equiv \mathbf{W}_{p} \mathbf{F}^{\dagger}, \quad \mathbf{W}_{\bar{F}} \equiv \mathbf{W}_{p} \bar{\mathbf{F}}^{\dagger}.$$
(14)

In analogy to what we did to derive the K-matrix representation of **S**, we now push \mathbf{W}_F through \mathbf{G}_{eff} to get $\mathbf{R}_{\text{in}} = (\mathbf{I}_{N_{\text{in}}} + i\mathbf{K}_F)/(\mathbf{I}_{N_{\text{in}}} - i\mathbf{K}_F)$, where $\mathbf{K}_F \equiv -\pi \mathbf{W}_F^{\dagger} \mathbf{\bar{G}}_0 \mathbf{W}_F$, and

 $\bar{\mathbf{G}}_0 \equiv [\mathbf{A}_0' - \mathbf{\Delta} + i\mathbf{\Gamma}_F]^{-1}$. The self-energies restricted to the input channels are

$$\Sigma_{F}^{R}(\omega) \equiv \Delta_{F}(\omega) - i\Gamma_{F}(\omega),$$

$$\Delta_{F}(\omega) \equiv \text{p.v.} \int d\omega' \frac{\mathbf{W}_{F}(\omega')\mathbf{W}_{F}^{\dagger}(\omega')}{\omega' - \omega},$$

$$\Gamma_{F}(\omega) \equiv \pi \mathbf{W}_{F}(\omega)\mathbf{W}_{F}^{\dagger}(\omega),$$
(15)

and similarly for \bar{F} . Taking the determinant of both sides of Eq. (14) and applying the same procedure used to derive Eq. (10), we get

$$\det \mathbf{R}_{\text{in}}(\omega) = \frac{\det \left(\mathbf{A}_0(\omega) - \mathbf{\Delta}(\omega) - i[\mathbf{\Gamma}_F(\omega) - \mathbf{\Gamma}_{\bar{F}}(\omega)]\right)}{\det \left(\mathbf{A}_0(\omega) - \mathbf{\Delta}(\omega) + i\mathbf{\Gamma}\right)},$$

where we have used Eq. (12) to write $\Gamma_F + \Gamma_{\bar{F}} = \Gamma$. Similar to Eq. (10), Eq. (16) relates the determinant of an $N_{\rm in}$ -by- $N_{\rm in}$ matrix to a ratio of functional determinants. Note that the denominator of Eq. (16) is the same as that of Eq. (10) while the numerators differ, implying that the poles (resonances) of $\mathbf{R}_{\rm in}$ are generically the same as those of \mathbf{S} , while zeros are different. (More precisely, all poles of $\mathbf{R}_{\rm in}$ are poles of \mathbf{S} , but there can exist special cases for which a pole of \mathbf{S} is not a pole of $\mathbf{R}_{\rm in}$, see the discussion below).

Equation (16) is a central result of this paper. It relates the *R*-zeros to a new effective operator:

$$\hat{A}_{RZ}(\omega) \equiv \hat{A}_0(\omega) - \hat{\Delta}(\omega) - i[\hat{\Gamma}_F(\omega) - \hat{\Gamma}_{\bar{F}}(\omega)]. \tag{17}$$

In particular, det $\mathbf{R}_{\text{in}}(\omega_{\text{RZ}}) = 0$ at an R-zero, so we necessarily have det $\hat{A}_{\text{RZ}}(\omega_{\text{RZ}}) = 0$, which defines a nonlinear eigenvalue problem:

$$\hat{A}_{RZ}(\omega_{RZ})|\omega_{RZ}\rangle = 0. \tag{18}$$

We expect that there exists a countably infinite set of R-zeros at complex frequencies $\{\omega_{RZ}\}$ that satisfy Eq. (18) for each choice of input channels F, similar to resonances, which satisfy $\hat{A}_{eff}(\omega_p)|\omega_p\rangle=0$. Like Eqs. (2) and (3), Eq. (18) is universal and applicable to any open system (with the caveat of short-ranged interactions) for any choice of reflectionless input channels. However, numerical solution of Eq. (18) can often be done more efficiently since \hat{A}_{RZ} varies slowly and smoothly as a function of the frequency ω . Implementation details for solving Eq. (18) in different geometries are given later in Sec. II F and Appendix B, where it is shown that the construction given here is equivalent to specifying modematched boundary conditions.

A caveat of using Eq. (18) as opposed to Eq. (2) is that while every R-zero corresponds to an eigenmode of \hat{A}_{RZ} in rare occasions some eigenmodes of \hat{A}_{RZ} may not be R-zeros. This can be seen from Eq. (16): det \mathbf{R}_{in} is not generally zero if both the numerator and the denominator on the right-hand side are zero, so that we have a simultaneous eigenmode of both \hat{A}_{RZ} and \hat{A}_{eff} . Such simultaneous eigenmodes are rare, but the aforementioned BIC [49] is an example, as pointed out in Ref. [48] in a more specialized context. In addition, resonances that do not radiate into certain channels [27,81,82]—sometimes referred to as "single-side resonances" or "unidirectional BICs"—are also such simultaneous eigenmodes; a single-side resonance is a pole \mathbf{S} but not

a pole of \mathbf{R}_{in} . BICs and single-side resonances require symmetry and/or additional parameter tuning beyond the basic RSM problem [49] since they have both zero incoming *and* zero outgoing waves in the dark channels.

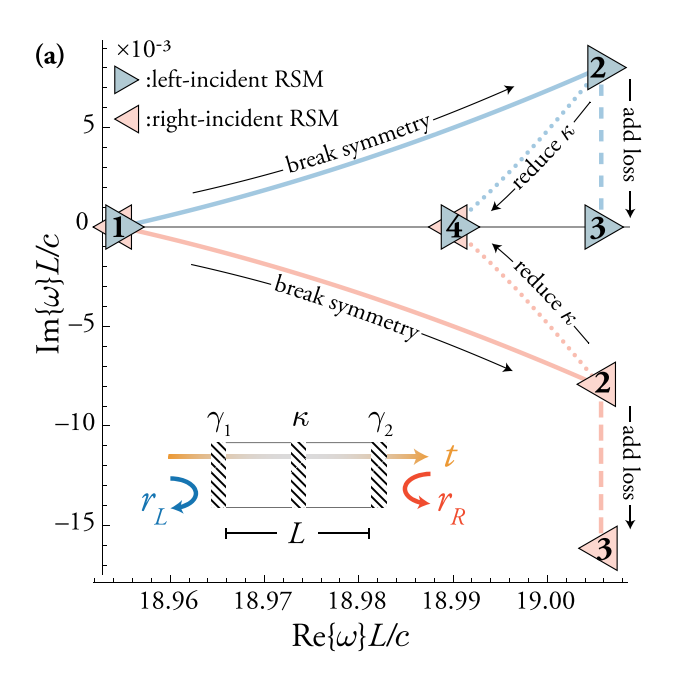
Equation (16) provides a rigorous basis for the topological-charge interpretation given earlier in Sec. II A. A topological defect of det $\mathbf{R}_{\rm in}(\omega)$ with charge +1 is an R-zero and is necessarily an eigenmode of $\hat{A}_{\rm RZ}$. Meanwhile, a topological defect of det $\mathbf{R}_{\rm in}(\omega)$ with charge -1 is a resonance and is necessarily an eigenmode of $\hat{A}_{\rm eff}$. When a +1 charge and a -1 charge annihilate, we have a simultaneous eigenmode of $\hat{A}_{\rm RZ}$ and $\hat{A}_{\rm eff}$, which is a BIC or a single-side resonance.

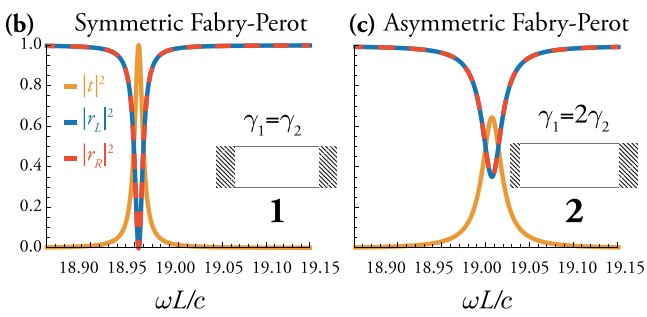
We note the important intuition provided by Eqs. (16)-(18): for the purpose of reasoning about the zeros of \mathbf{R}_{in} , each input channel acts as an effective "radiative gain" to the system (because it contributes a negative semidefinite term to \hat{A}_{RZ} , which then increases the imaginary part of its eigenvalue ω_{RZ}), and each output channel as an effective "radiative loss." The balance of these two terms will determine the proximity of an R-zero to the real-frequency axis, where it becomes an RSM. Hence when defining an R-zero problem in which few input channels scatter to many output channels, we expect the R-zero frequency to appear in the lower half of the complex plane for a passive system (similar to resonances). Therefore to realize a steady-state solution we can either add gain in the dielectric function of the operator \hat{A}_0 (gain-loss engineering) or modify the scattering structure to increase the coupling of the input channels (index tuning) so as to move the solution to a real frequency. In the opposite case of many more input channels than output channels, we expect the R-zero frequency to appear in the upper half-plane and require adding absorption or increased coupling to the output channels to reach the real axis. This argument is merely qualitative, since the operator in Eq. (17) is the sum of noncommuting terms, so that the imaginary part of the eigenvalue is not simply the sum of contributions from each term. However this qualitative picture is confirmed by the approximate coupled-mode analysis of Sec. IIE and by exact numerical solutions of several examples (see Figs. 2, 5, and 6).

As noted above, there is an important difference between the zeros of S and of $R_{\rm in}$. Flux conservation means that the totally absorbed steady-state CPA cannot be realized without introducing absorption. On the other hand, flux conservation does not prevent the existence of R-zeros on the real axis (RSMs) since the incident flux can be redirected to the \bar{F} output channels. Mathematically, S is unitary for lossless systems at real frequencies, with unimodular eigenvalues, but $R_{\rm in}$ is not, and may have a zero even for real frequency. This is why RSMs can be achieved via pure index tuning, even though CPA and lasing cannot; we will give explicit examples later [Figs. 2(e), 5, and 6].

D. Symmetry properties of R-zeros and RSMs

We now analyze exact properties of *R*-zeros and RSMs under time reversal and discrete spatial transformations, in the presence of symmetries with respect to these transformations. An earlier work [37] studied the consequences of symmetry in one dimension, and has some overlap with what follows,





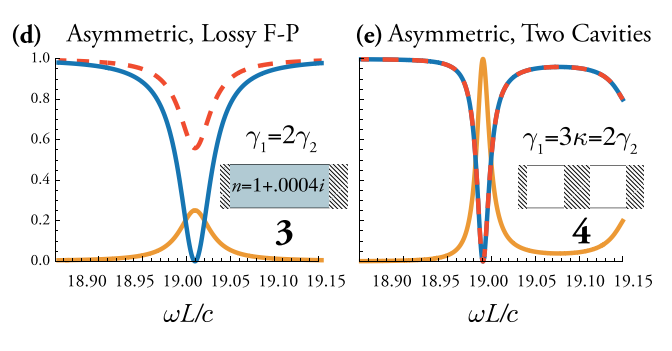


FIG. 2. Illustration of RSMs and R-zero spectrum for simple two- and three-mirror resonators of length L in one dimension, consisting of δ -function mirrors of strengths γ_1^{-1} , γ_2^{-1} , and κ^{-1} , as indicated in the schematic in (a). Throughout, we fix $\gamma_2 \equiv c/L$. Blue and red lines $1 \to 2$ indicate the effect of breaking symmetry by varying γ_1 from $\gamma_2 \to 2\gamma_2$. A bidirectional RSM [as in (b)] splits into two complex-conjugate R-zeros off the real axis and a reflectionless steady-state (RSM) no longer exists, as in (c). Adding absorption to the cavity, indicated by blue and red lines $2 \to 3$, brings the upper R-zero to the real axis (but not the lower one), creating a unipolar left-incident lossy RSM, as in (d). Alternatively, adding a middle mirror and reducing its κ from $\infty \to 2\gamma_2/3$ is sufficient to bring both R-zeros back to the real axis $[2 \to 4$ in (a)], creating a bipolar RSM at a different frequency from the symmetric Fabry-Pérot resonator [see (e)], without restoring parity symmetry.

though the present treatment generalizes to any dimension, and applies to complex *R*-zeros, not only real RSMs.

1. Time-reversal transformation (\mathcal{T}) and symmetry

The action of time reversal (\mathcal{T}) is to complex conjugate everything, including the wave operators \hat{A} and \hat{A}_{RZ} , and the field $\mathbf{H}(\mathbf{r})$. This interchanges the input and output channels $(F \leftrightarrow \bar{F})$:

$$\mathcal{T}: (\omega, \varepsilon(\mathbf{r}), F) \to (\omega^*, \varepsilon^*(\mathbf{r}), \bar{F}).$$
 (19)

It follows that if a cavity with dielectric function $\varepsilon(\mathbf{r})$ has an R-zero at frequency ω_0 with input channels given by F, then the cavity with $\varepsilon^*(\mathbf{r})$ has an R-zero at frequency ω_0^* with input channels given by the complement, \bar{F} .

The cavity or scatterer is said to have time-reversal symmetry when $\varepsilon(\mathbf{r}) = \varepsilon^*(\mathbf{r})$, i.e., when there is no absorption or gain. In such case, the "two cavities" described above are the same, and we can conclude that complementary R-zeros come in complex-conjugate pairs for flux-conserving (passive) cavities. This is true independently of the presence or absence of spatial symmetries, such as parity. The system can then be tuned to have an RSM either by index tuning or by gainloss tuning. In the former case, the new cavity still exhibits time-reversal symmetry, so the resulting RSM is bipolar, by which we mean that a complementary RSM exists at the same frequency; examples are given in Figs. 2(b), 2(e), 5, and 6. In the case of gain-loss tuning, the new cavity no longer exhibits time-reversal symmetry, and we do not expect another RSM at that frequency; we refer to this as unipolar (this is the generalization of unidirectional reflectionless states for the 1D \mathcal{PT} cases mentioned above).

In Fig. 2(a) we illustrate the concept of tuning to create an RSM for the simple case of an asymmetric Fabry-Pérot cavity. We start with a symmetric Fabry-Pérot cavity, which has both \mathcal{P} and \mathcal{T} symmetry (this symmetry class will be discussed in more detail in Sec. II D 5); it is well known that such a cavity has equally spaced unit-transmission resonances [83], which we refer to as bidirectional RSMs [see Fig. 2(b)]. We break parity symmetry but maintain the \mathcal{T} symmetry by making the mirror reflectivities unequal [Fig. 2(a) solid lines]; as a consequence there is no longer an RSM for either direction of incidence at any real frequency [Fig. 2(c)]. However, there is now a pair of complex-conjugate R-zeros off the real axis, as demanded by the \mathcal{T} symmetry. Here we have made the left barrier less reflective than the right one, and we observe that the left-incident R-zero has moved to the upper half-plane and the right-incident R-zero to the lower half-plane, which is consistent with the intuition given in Sec. II C.

One way to recover the RSMs without restoring parity symmetry is to use gain-loss engineering (non-Hermitian tuning). Again the intuitive picture of Sec. II C suggests that adding absorption will reduce the imaginary parts of the *R*-zero frequencies, which can be used to create a left-incident RSM. A physical argument supporting this conclusion is that when the mirror reflectivities are equal the prompt reflection from either mirror is canceled by the total left or right reflection of waves reaching the interior and internally reflecting an odd number of times before escaping back in the incident

direction. When the left mirror is less reflective than the right one, its prompt reflection is decreased and the internal reflection backwards is increased, so total destructive interference is not possible. However, if one adds the right amount of absorption to the interior, these two amplitudes can again be balanced and destructive interference in the backwards direction can be restored with tuning of the frequency. This change has the opposite effect on a right input wave, making destructive interference impossible for the same parameters, and leading to a unipolar left-incident RSM. For a right-incident RSM one would instead have to add the same amount of gain to the interior. This physical picture is confirmed by Fig. 2(a) dashed lines and Fig. 2(d).

Alternatively, we can employ index tuning to create an RSM, in this case by adding a third lossless mirror in the interior. We can think of the left region and the interior mirror as forming a composite mirror such that for some mirror reflectivity and input frequency left and right escape is again balanced. Indeed such a three-mirror system does have an RSM with one-parameter tuning as shown by Fig. 2(a) dotted lines and Fig. 2(e). Moreover, as the system is flux conserving and reciprocal, it must be a bipolar RSM. Comparison of Figs. 2(a), 2(d) and 2(e) illustrates this important difference between the two types of tuning: for the lossless case, both left- and right-incident *R*-zeros maintain their complex conjugate relation as the interior mirror is tuned and hence meet on the real axis.

2. Parity transformation (P) and symmetry

Consider a parity transformation \mathcal{P} satisfying $\hat{\mathcal{P}}^2 = \hat{1}$ and det $\mathcal{P} = -1$. Common examples of parity are reflections (e.g., $x \to -x$) and inversion in three dimensions $(x \to -x, y \to -y, z \to -z)$.

Generally, the action of \mathcal{P} is to leave the frequency unchanged and to map $\varepsilon(\mathbf{r}) \to \varepsilon(\mathcal{P}\mathbf{r})$, $\mathbf{H}(\mathbf{r}) \to \mathbf{H}(\mathcal{P}\mathbf{r})$, relating an R-zero-RSM of one structure to that of a structure transformed by \mathcal{P} . However, these two *R*-zeros are generally not complementary to each other. Therefore, we further require the input-output channels to have P symmetry, by which we mean that $\varepsilon(\mathbf{r}) = \varepsilon(\mathcal{P}\mathbf{r})$ in the asymptotic region and that the input channels are chosen such that F maps to \bar{F} under \mathcal{P} ; we call this a "bisected" partition of the channels. The most common bisected systems would be those that naturally divide into "left" and "right" and for which the input channels are chosen to be all left or all right channels, which generalizes the well-studied one-dimensional case. But there are also other possibilities, e.g., a partition into clockwise and counterclockwise channels for a finite-sized scatterer in free space. For a bisected partition F, the action of \mathcal{P} is

$$\mathcal{P}: (\omega, \varepsilon(\mathbf{r}), F) \to (\omega, \varepsilon(\mathcal{P}\mathbf{r}), \bar{F}).$$
 (20)

When an *R*-zero with a bisected partition is bipolar, we refer to it as *bidirectional*; when it is unipolar, we refer to it as *unidirectional*.

We say that the cavity or scatterer has \mathcal{P} symmetry when $\varepsilon(\mathbf{r}) = \varepsilon(\mathcal{P}\mathbf{r})$, for which we can say that when the cavity and the channel partition both have \mathcal{P} symmetry R-zeros are bidirectional, whether or not $\omega_{RZ} \in \mathbb{R}$. This is in contrast to

the case with \mathcal{T} symmetry, where bipolarity only holds for real-frequency RSMs.

3. Parity-time transformation (PT), symmetry, and symmetry-breaking transition

The action of the joint parity-time (\mathcal{PT}) operator, i.e., performing both \mathcal{P} and \mathcal{T} transformations simultaneously, is particularly interesting as it is the case of \mathcal{PT} symmetry that brought recent attention to unidirectional RSMs. We assume that the asymptotic region has \mathcal{P} symmetry and that the partition F is bisected; hence the action of \mathcal{PT} is

$$\mathcal{PT}: (\omega, \varepsilon(\mathbf{r}), F) \to (\omega^*, \varepsilon^*(\mathcal{P}\mathbf{r}), F).$$
 (21)

When the scattering region has \mathcal{PT} symmetry, namely, when $\varepsilon^*(\mathcal{P}\mathbf{r}) = \varepsilon(\mathbf{r})$, such systems either have unidirectional RSMs with $\omega_0 \in \mathbb{R}$ or complex-conjugate pairs of unidirectional R-zeros of the *same directionality* with $\omega_0 \in \mathbb{C}$. This is in contrast to the case of \mathcal{T} symmetry alone, which allows real bidirectional RSMs or complex-conjugate pairs of R-zeros of *opposite* polarity or directionality.

This property of the PT case implies something quite important. Often PT scattering systems are studied by beginning with a flux-conserving system (satisfying both P, Tsymmetries separately) and adding gain and absorption antisymmetrically so as to break $\mathcal P$ and $\mathcal T$ symmetries while preserving \mathcal{PT} . The initial system has bidirectional RSMs, i.e., a degenerate pair of left and right RSMs (see discussion of the \mathcal{P} , T case below in Sec. II D 5) but has no other degeneracy; thus the left and right RSMs are constrained to remain on the real axis as unidirectional RSMs when the value of the gain-loss strength increases. (If, e.g., a left-incident RSM moved off the real axis immediately, it would lack a second left-incident RSM as complex-conjugate partner, violating the condition above.) These unidirectional RSMs are invariant under the PT transformation, so they are said to be in the PTunbroken phase. As the gain-loss strength is further increased, eventually each RSM may meet another RSM of the same directionality at a real frequency [see Fig. 3(b) below as an example], above which point, generically, the pair of RSMs will leave the real axis as complex-conjugate pairs of R-zeros, becoming inaccessible in steady state. These complex-conjugate pairs of R-zeros do not exhibit PT symmetry (one maps to its conjugate partner under the PT transform), so they are said to be in the PT-broken phase. The above explains the commonly observed RSMs in 1D systems with PT symmetry [13,21-24,26,27] or anti- \mathcal{PT} symmetry [84] and their disappearance at large gain-loss parameters [22-25,37]. It should be noted that the critical parameters that define the PT transitions are different for each RSM pair and different for each directionality. They are also different from the transitions where a pair of unimodular eigenvalues of the S matrix turn into an amplifying one and an attenuating one [24,85].

This behavior is illustrated for the one-dimensional $\mathcal{P}T$ symmetric structure shown in Fig. 3(a): an etalon of thickness L in air where the left half has refractive index $n = n_1 - in_2$ and the right half has index $n = n_1 + in_2$. For a passive etalon $(n_2 = 0)$, bidirectional RSMs exist at real frequencies $\omega_{\text{RSM}} = m\pi c/n_1 L$ with $m \in \mathbb{Z}$. When the gain-loss strength n_2 is

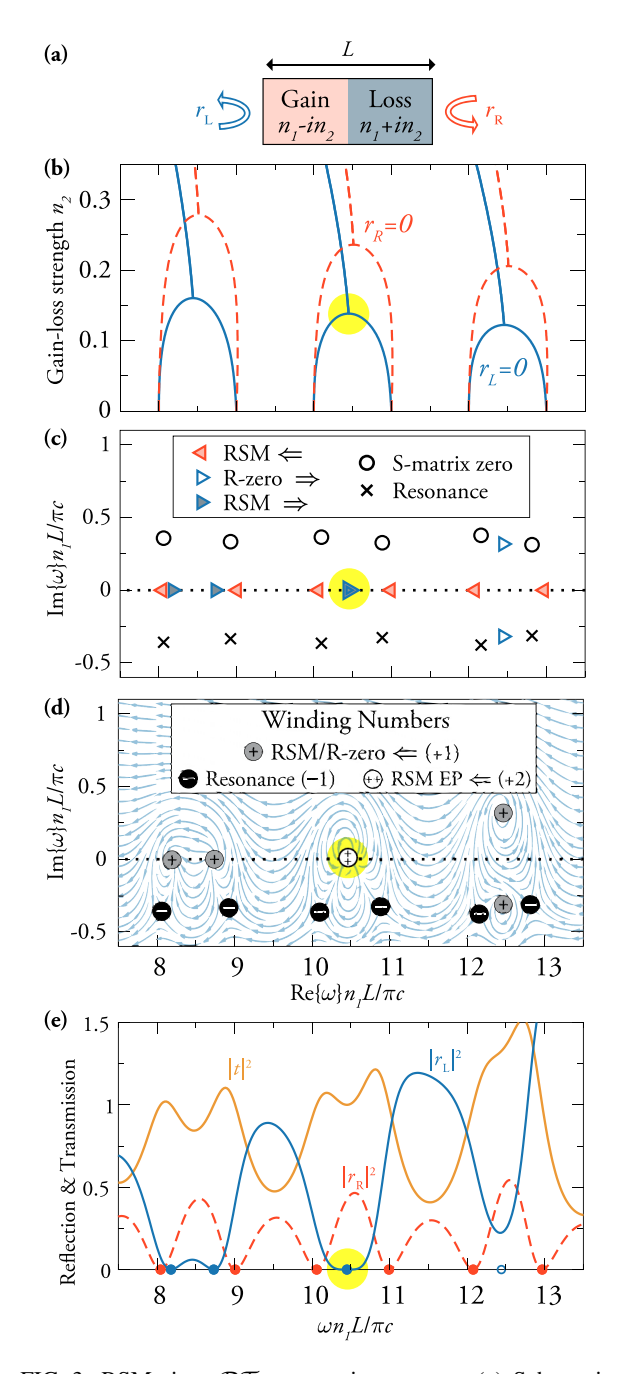


FIG. 3. RSMs in a \mathcal{PT} -symmetric structure. (a) Schematic of the structure: an etalon in air, with refractive index $n = n_1 - in_2$ on the left and $n = n_1 + in_2$ on the right; here $n_1 = 2$. (b) Real part of the R-zero frequencies (blue solid lines, left-incident; red dashed lines, right-incident) as the gain-loss strength is increased. For small n_2 , the frequencies are real valued. After two RSMs meet at an RSM EP (highlighted in yellow), they split into two R-zeros at complexconjugate frequencies. (c) Spectra of the R-zeros and RSMs, S-matrix zeros, and resonances in the complex-frequency plane at $n_2 = 0.13844$ where two right-going RSMs meet. (d) Streamlines of the vector field (Re (r_L) , Im (r_L)), showing +1 topological charges at R-zeros and RSMs and -1 topological charges at resonances. When two RSMs meet at an RSM EP, the topological charges add up to +2. (e) Reflection and transmission spectra at the same n_2 as in (c) and (d); blue and red filled dots mark the RSM frequencies, and the open blue dot is the real part of complex R-zero, which has already crossed the threshold.

increased, pairs of RSMs move toward each other in frequency as shown in Fig. 3(b). As parity and time-reversal symmetries are individually broken, the right-incident RSMs (for which $r_{\rm R}=0$) and the left-incident RSMs (for which $r_{\rm L}=0$) now occur at different frequencies. But since the system still exhibits \mathcal{PT} symmetry, all of these RSM frequencies remain real-valued. At critical values of n_2 , a pair of RSMs meet. As n_2 is further increased, the pair of RSMs split into two, leaving the real-frequency axis as complex-conjugate pairs of R-zeros. The RSM spectrum in the complex-frequency plane, together with the S-matrix zeros and poles (resonances), is shown in Fig. 3(c) for a critical value of n_2 where two right-going RSMs meet. The corresponding reflection and transmission spectra are given in Fig. 3(e).

We use this example to illustrate the topological properties of R-zeros–RSMs and resonances. Figure 3(d) shows the streamlines of the vector field (Re(r_L), Im(r_L)) in the complex-frequency plane. Following the discussion in Sec. II A, we indeed observe that $\arg(r_L)$ winds by 2π along counterclockwise loops around each R-zero or RSM (corresponding to a +1 topological charge), while it winds by -2π around each resonance (corresponding to a -1 topological charge). When two RSMs meet, they superpose as one topological defect with charge +2, as highlighted in yellow. We further discuss such a coalescence of RSMs in the next section.

4. RSM exceptional points

Non-Hermitian operators have the property that when two eigenvalues become degenerate (in both their real and imaginary parts) the two associated eigenvectors also coalesce into one. Such a coalescence is called an EP in parameter space and has many unique properties [17-20,86,87]. EPs of the purely outgoing (resonance) wave operator have been widely studied [88-98], and recently so too have EPs of the purely incoming wave operator with $\mathcal{P}T$ symmetry [99] or unconstrained by any symmetry [100].

The R-zero-RSM wave operator \hat{A}_{RZ} of Eq. (17) is non-Hermitian and shares many similarities with the purely outgoing (resonance) wave operator \hat{A}_{eff} . It is therefore possible to create RSM exceptional points where multiple reflectionless states coalesce into one, which is, from a physical point of view, a kind of EP not previously studied (to our knowledge). The aforementioned RSM transitions in PT systems are examples of this. These RSM EPs share some common features with the perfectly absorbing EPs of Refs. [99,100]. In particular, there is no self-oscillating instability (lasing) when the EP reaches the real axis; a steady-state RSM EP is compatible with linear response. At an RSM EP, the line shape of the reflection intensity will change from its generic quadratic form to a quartic, flat-bottomed line shape, characteristic of a +2 topological charge. An example of this effect is shown in Figs. 3(d)-3(e), where the RSM EP is highlighted in yellow. Near an EP of any kind, the complex eigenvalue typically exhibits a square-root dependence on system parameters, visible in Fig. 3(b).

Note that RSMs in one-dimensional systems have been characterized in some works as EPs of an unconventional non-symmetric scattering matrix [26,36,37,40,101–103]. How-

TABLE I. Consequences of discrete symmetries for the RSM problem. F is the set of input states. Unipolar means that only one set of input channels has zero reflection at a given frequency and bipolar means that its complement does too. In this table we assume that the channels are bisected, i.e., the set of input channels maps to its complement under a parity transformation \mathcal{P} . In this case we use the terms unidirectional instead of unipolar, and bidirectional instead of bipolar. N_{RSM} is the minimum number of system parameters that must be tuned (consistent with symmetry) to achieve an RSM (i.e., make ω_F real), while $N_{\text{RSM}}^{\text{EP}}$ parameters are necessary for an exceptional point of RSMs (i.e., degenerate real ω_{RZ}).

Symmetry type	$\varepsilon(\mathbf{x})$ same as	ω_F pairs with	RSM type $(\omega_F \in \mathbb{R})$	$N_{ m RSM}$	$N_{ m RSM}^{ m EP}$	$\mathbb{R} \to \mathbb{C}$ transition?
None			Unipolar	1	3	×
$\mathcal T$	$\varepsilon^*(x)$	$\omega_{ar{c}}^*$	Bipolar	1	3	X
${\cal P}$	$\varepsilon(\mathcal{P}\boldsymbol{x})$	$\omega_{ar{F}}^{r}$	Bidirectional	1	3	X
$\mathcal{P}T$	$\varepsilon^*(\mathcal{P}x)$	ω_F^*	Unidirectional	0/1	1	\checkmark
\mathcal{P}, T	$\varepsilon^*(x),$ $\varepsilon(\mathcal{P}x)$	$\omega_{ar{F}},\ \omega_{ar{F}}^*,\omega_F^*$	Bidirectional	0/1	1	√

ever, those are nondegenerate RSMs and are not EPs of the underlying wave operator. Also, in higher dimensions, an EP of this unconventional nonsymmetric scattering matrix is no longer a reflectionless state. Therefore, we do not adopt this convention and reserve the term "RSM EP" for the states discussed in this section.

5. \mathcal{P} and \mathcal{T} symmetry and symmetry-breaking transition

The final symmetry class we will discuss is the case of systems with both $\mathcal P$ and $\mathcal T$ symmetries. Here we must make a further remark for clarity. Up to now we have only discussed the implications of symmetries of the scatterer or cavity and its channels, but not the full symmetry of the wave operator for RSMs. Even if a cavity and leads have \mathcal{P} and \mathcal{T} symmetry, the RSM boundary condition breaks \mathcal{P} symmetry and the RSM solutions can have at most PT symmetry, as noted in Ref. [48] (although they did not discuss cavities with PT symmetry). The symmetric lossless Fabry-Pérot cavity, discussed briefly above, is a familiar example of a system with both \mathcal{P} and \mathcal{T} . Such a \mathcal{P} , T system simultaneously exhibits all of the symmetry properties given in Secs. IID 1–IID 3. Therefore we can expect bidirectional RSMs on the real-frequency axis without any tuning, with flux conservation implying unit transmission for these RSMs, as is indeed the case for the Fabry-Pérot. However there is another possibility allowed by the symmetry: bidirectional complex-conjugate pairs of R-zeros. Such pairs do not arise for the Fabry-Pérot or other "two-mirror" resonators. but we have found that they do exist for multimirror resonators. In fact starting with a two-mirror 1D resonator and introducing a third middle mirror we have confirmed that we can induce a symmetry-breaking transition in which pairs of bidirectional RSMs meet on the real axis at two degenerate EPs, and then move off the real axis as bidirectional complex-conjugate pairs of R-zeros. Moreover, one can show that this transition is actually associated with PT-symmetry breaking, despite the absence of gain or absorption. We will defer detailed discussion of this interesting case to a future paper [104].

The different symmetry classes and their properties are summarized in Table I and Fig. 4. Similar conclusions were reached for the special case of two-channel structures in quantum transport in Ref. [105].

E. Coupled-mode analysis

The preceding results were derived directly from Maxwell's equations and involve no approximation. Meanwhile, in many circumstances an approximate analytic model will be adequate and desirable for simplicity. In photonics a standard tool is the temporal coupled-mode theory (TCMT) [51,106–110], which is a phenomenological model widely used in the design and analysis of optical devices [16,93,111,112]. The TCMT formalism is derived from symmetry constraints [51,106–109] rather than from first principles, yet it leads to an analytic relation between the scattering matrix and the underlying Hamiltonian that is similar to Eq. (8) and is reasonably accurate in many cases. Assuming harmonic time dependence, a reciprocal cavity or scattering region supporting M internal resonances and coupled to 2Nexternal channels (N incoming and N outgoing) can be described by [107]

$$-i\omega \mathbf{a} = -i\mathbf{H}_{\text{eff}}\mathbf{a} + \mathbf{D}^T\boldsymbol{\alpha}, \qquad (22a)$$

$$\boldsymbol{\beta} = \mathbf{S}_0 \boldsymbol{\alpha} + \mathbf{D} \mathbf{a},\tag{22b}$$

where $\mathbf{H}_{\mathrm{eff}}$ is an M-by-M effective Hamiltonian

$$\mathbf{H}_{\text{eff}} \equiv \mathbf{H}_{\text{close}} - i \frac{\mathbf{D}^{\dagger} \mathbf{D}}{2}, \tag{23}$$

and a is a column vector containing the field amplitudes of the M resonances. The N-by-M matrix \mathbf{D} contains the coupling coefficients between the resonances and the channels; the mth column of \mathbf{D} is essentially the radiation wavefront of the mth resonance analyzed in the channel basis. The Hamiltonian matrix \mathbf{H}_{close} describes a closed system and is Hermitian in the absence of absorption or gain; $(\omega - \mathbf{H}_{close})$ is analogous to A_0 in Eq. (6) or $A'_0 - \Delta$ in Eq. (9); the frequency shifts Δ due to openness are not separately included in TCMT. The positive semidefinite matrix $\mathbf{D}^{\dagger}\mathbf{D}/2$ is analogous to Γ in Eq. (9); its diagonal elements are the decay rates of the modes due to radiation into channels in the open environment, and its off-diagonal elements are the dissipative via-the-continuum coupling rates. The "direct scattering matrix" $\mathbf{S}_0 = \mathbf{S}_0^T$ is symmetric and describes the "nonresonant" part of the scattering process that varies slowly with frequency. The distinction between "resonant" and "nonresonant" is not always clear; the typical practice in TCMT is

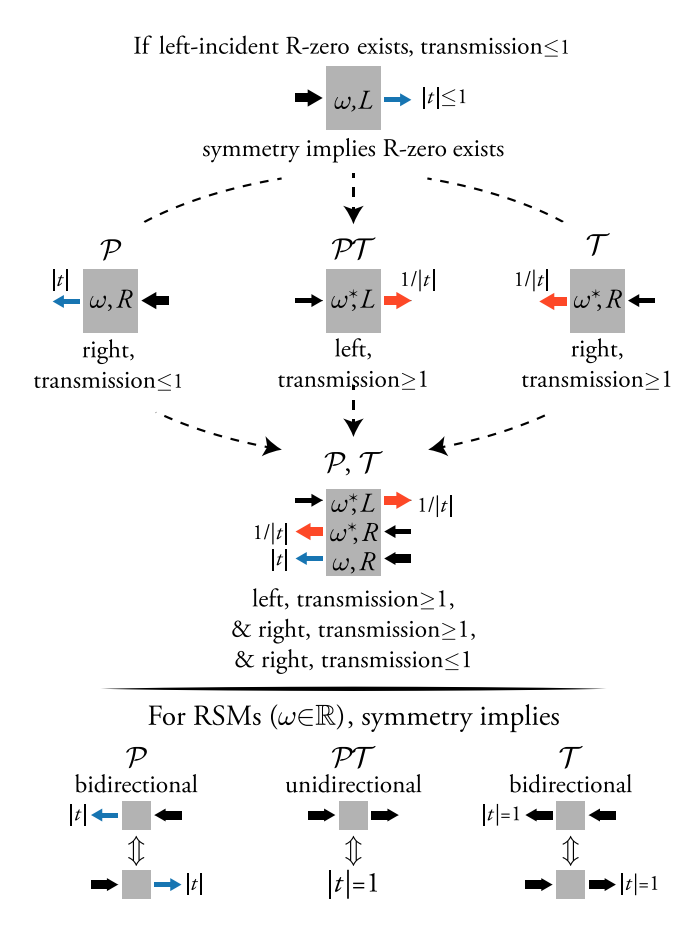


FIG. 4. (Color) Schematic illustrating the implications of symmetry for R-zeros and RSMs. Top: Beginning with the assumption of the existence of a left-incident R-zero with transmission |t| < 1 at some frequency, ω , there will exist other R-zeros with specific properties based on the presence of $\mathcal{P}, \mathcal{T}, \mathcal{PT}$ symmetry (as shown by arrows). Bottom: The initial state has real frequency (is an RSM), which exists in steady state; the implications of the various symmetries are shown for this case. Note that if ω is real the implications for the \mathcal{T} and $(\mathcal{P}, \mathcal{T})$ are the same: bidirectional unit transmission reflectionless states.

to use \mathbf{H}_{close} and \mathbf{D} to model one or a few high-quality-factor resonances in the frequency range of interest, and bundle the contributions from the further-away and/or low-quality-factor resonances into \mathbf{S}_0 in an empirical manner. In a passive system without absorption or gain, time-reversal symmetry requires that $\mathbf{S}_0\mathbf{D}^* = -\mathbf{D}$ (Refs. [107,109]); here we assume that the possible presence of absorption or gain can be modeled through an anti-Hermitian term in \mathbf{H}_{close} without breaking the $\mathbf{S}_0\mathbf{D}^* = -\mathbf{D}$ condition. It follows that the scattering matrix is

$$\mathbf{S}(\omega) = \left(\mathbf{I}_N - i\mathbf{D}\frac{1}{\omega - \mathbf{H}_{\text{eff}}}\mathbf{D}^{\dagger}\right)\mathbf{S}_0,\tag{24}$$

where \mathbf{I}_N is the *N*-by-*N* identity matrix. When all contributing resonances (including the low-quality-factor ones that may be far away in frequency) are included in $\mathbf{H}_{\text{close}}$ and \mathbf{D} , the direct scattering matrix will be simply $\mathbf{S}_0 = \mathbf{I}_N$ [110]. The similarity between Eqs. (8) and (24) is evident. A formalism mathematically equivalent to TCMT is also used in quantum noise theory [113].

From Eq. (24), one may proceed to derive an expression for the determinant of the generalized reflection matrix similar to Eq. (16); we leave such an exercise to the interested readers, and instead provide an alternative approach here. Let us define $\mathbf{D}_{\text{in}} \equiv \mathbf{F}\mathbf{D}$, using the filtering matrix \mathbf{F} introduced earlier, as the coupling coefficients into the N_{in} input channels defining F, and similarly \mathbf{D}_{out} as the coefficients to the output channels. Consider $\mathbf{S}_0 = \mathbf{I}_N$. Using Eq. (13), Eq. (24), and the Woodbury matrix identity [114], we can write the inverse of the generalized reflection matrix as

$$\mathbf{R}_{\text{in}}^{-1}(\omega) = \mathbf{I}_{N_{\text{in}}} + i\mathbf{D}_{\text{in}} \frac{1}{\omega - \mathbf{H}_{\text{RZ}}} \mathbf{D}_{\text{in}}^{\dagger}, \tag{25}$$

where we have defined a matrix

$$\mathbf{H}_{RZ} \equiv \mathbf{H}_{close} + i \frac{\mathbf{D}_{in}^{\dagger} \mathbf{D}_{in}}{2} - i \frac{\mathbf{D}_{out}^{\dagger} \mathbf{D}_{out}}{2}.$$
 (26)

The matrix $(\omega - \mathbf{H}_{RZ})$ is analogous to $\hat{A}_{RZ}(\omega)$ in Eq. (17). At the frequency $\omega = \omega_{RZ}$ of an R-zero, $\det(\mathbf{R}_{in}^{-1}) = 1/\det(\mathbf{R}_{in})$ diverges, and Eq. (25) shows that such divergence can only happen when ω is an eigenvalue of \mathbf{H}_{RZ} . Therefore, every R-zero is necessarily an eigenmode of \mathbf{H}_{RZ} . Note, however, that the reverse is not true: not every eigenmode of \mathbf{H}_{RZ} is an R-zero, since it is possible for $||\mathbf{D}_{in}(\omega - \mathbf{H}_{RZ})^{-1}\mathbf{D}_{in}^{\dagger}|| < \infty$ even when ω is an eigenvalue of \mathbf{H}_{RZ} ; this happens when the eigenmode \mathbf{a} satisfies $\mathbf{D}_{in}\mathbf{a} = 0$, which is precisely when it is a BIC or a one-sided resonance—see discussions at the end of Sec. II C.

Like \hat{A}_{RZ} , the matrix \mathbf{H}_{RZ} can be understood intuitively. Outgoing radiation into the N_{out} output channels introduces an effective radiative loss term $-i\mathbf{D}_{\text{out}}^{\dagger}\mathbf{D}_{\text{out}}/2$. Incident light coming from the N_{in} input channels introduces an effective "radiative gain" term $+i\mathbf{D}_{\text{in}}^{\dagger}\mathbf{D}_{\text{in}}/2$.

The case when there is only one dominant resonance in the frequency range of interest (M=1) is particularly instructive. Here, $\mathbf{H}_{\text{close}} = \omega_0 - i\gamma_{\text{nr}}$ is a scalar where γ_{nr} is the nonradiative decay rate due to absorption or gain, and the *R*-zero frequency given by Eq. (26) is

$$\omega_{\text{RZ}} = (\omega_0 - i\gamma_{\text{nr}}) + i(\gamma_{\text{in}} - \gamma_{\text{out}}),$$

$$\gamma_{\text{in}} \equiv \sum_{n \in F} |d_n|^2 / 2, \quad \gamma_{\text{out}} \equiv \sum_{n \notin F} |d_n|^2 / 2,$$
(27)

where d_n is the coupling coefficient (partial width) of the mode to the nth channel.

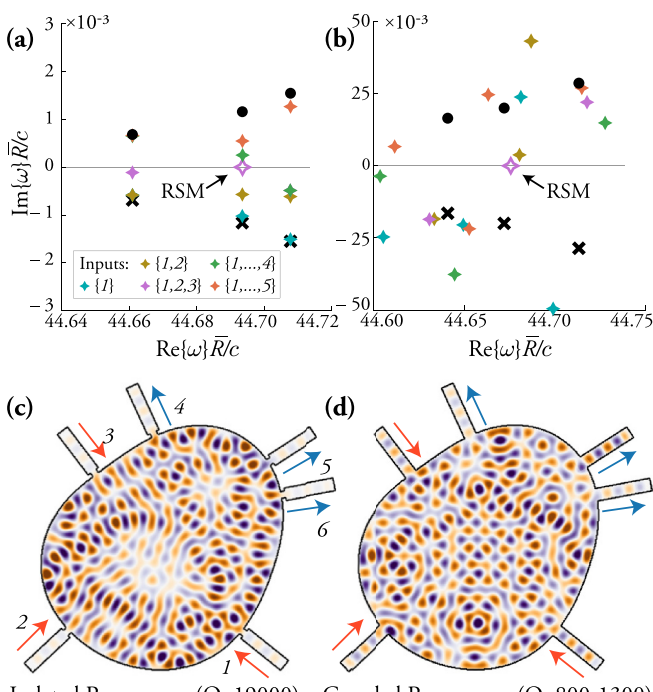
In this single-mode approximation, which is widely used in the context of high-Q resonant structures, the intuitive understanding of RSMs as generalized critical coupling is realized. Since only one resonance is relevant one can speak of the total coupling into and out of the system as a scalar quantity. The total in-coupling rate for the input channels acts as an effective source of gain, while the total decay rate into the output channels plus the intrinsic absorption in the cavity act as an effective loss. When these two quantities are equal (critical coupling), the reflectionless state has a real frequency and becomes an RSM. Within this approximation there are no multiresonance pushing or pulling effects or other sources of real-frequency shifts. Therefore all the different R-zero boundary conditions simply move the frequency of the corresponding R-zero vertically in the complex plane between the

purely outgoing solution (resonance) in the lower half-plane and the purely incoming solution (S-matrix zero) in the upper half-plane. (The picture is trivially changed in the presence of absorption in the cavity, as the S-matrix resonance and zero move rigidly down and are no longer symmetric around the real axis.) It is straightforward to also show that the RSM incident wavefront α_{RSM} is simply the phase conjugation of the resonance's radiation wavefront into the designated channels. When $\omega = \omega_{RZ}$, the nonresonant reflection α_{RSM} is exactly canceled by the resonant scattering \mathbf{Da} back into those channels. When the frequency is detuned from ω_{RZ} , the reflection signal rises as a Lorentzian function with the linewidth being that of the underlying resonance, $(\gamma_{in} + \gamma_{out} + \gamma_{nr})$.

The single-resonance scenario is the simplest example of an *R*-zero, yet it already explains the impedance-matching conditions previously found using TCMT in waveguide branches [115], antireflection surfaces [116], and polarization-converting surfaces [62]: i.e., that zero reflection in a passive ($\gamma_{nr}=0$) system is achieved at ω_0 when the decay rate into the incident channel γ_{in} equals the sum of decay rates into all outgoing channels γ_{out} .

The single-resonance approximation is typically valid when a cavity has a high-quality factor (Q) and is weakly coupled to the input-output channels, so that its resonances are near the real axis and multiresonance effects can be neglected at most frequencies. However the general RSM theory applies equally well to low-Q cavities where the simple picture just described breaks down substantially. Yet the full theory of RSM guarantees the existence of R-zeros and the possibility of tuning them to be RSMs, even if the scattering is through multiple overlapping resonances. An example of both limits is given in Fig. 5, where we study, using an exact numerical method, an asymmetric resonant cavity connected to six single-mode waveguides. The cavity shown in Fig. 5(c) has constrictions at its waveguide junctions to increase the quality factors of the resonances. In Fig. 5(a) we show the R-zero spectrum for this cavity, which has the vertical clustering bracketed by the resonance and S-matrix zero, as predicted by the single resonance approximation just discussed. In contrast, the cavity shown in Fig. 5(d) has the constrictions opened, which increases the quality factors by a factor of ≈ 20 . For this case the single-resonance approximation fails, and the R-zero spectrum [Fig. 5(b)] is spread out in both the real and imaginary-frequency axes. Strikingly, some R-zeros lie below the resonances while others lie above the S-matrix zeros in the complex-frequency plane, something which is forbidden within the single resonance approximation. Nonetheless, in both cases, we were able to tune to a real-frequency RSM for the three-in, three-out boundary condition simply by slightly varying the constrictions of the outgoing waveguides. As noted above this shows that the full RSM theory developed here is a major advance over previous theories based on the concept of critical coupling through a single resonance and will work also for open cavities, where multiresonance effects dominate.

When $\mathbf{S}_0 \neq \mathbf{I}_N$, the TCMT analysis above shows that each ω_{RZ} is an eigenfrequency of $\mathbf{H}_{RZ} \equiv \mathbf{H}_{eff} + i\mathbf{D}^{\dagger}\mathbf{S}_0\mathbf{F}^{\dagger}(\mathbf{F}\mathbf{S}_0\mathbf{F}^{\dagger})^{-1}\mathbf{F}\mathbf{D}$. In the case where $\mathbf{F}\mathbf{S}_0\mathbf{F}^{\dagger}$ is not invertible, we can instead apply Eqs. (25) and (26) to $\mathbf{S}\mathbf{S}_0^{-1}$ (instead of directly to \mathbf{S}). In this case the "reflectionless" mode



Isolated Resonances (Q~19000) Coupled Resonances (Q~800-1300)

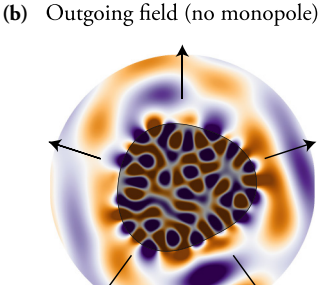
FIG. 5. Asymmetric lossless waveguide junction and resonator (mean radius \bar{R}) coupled to six single-mode waveguides, with constrictions at the entrances to the junction. (a) Numerically calculated R-zero spectrum for a weakly coupled, high-Q junction with well-isolated resonances. The black x and dot are purely outgoing (resonance) and incoming (S-matrix zero) frequencies, which are complex conjugates. Colored stars are R-zeros for various choices of input channels; the legend indicates which channels are inputs, with the channel labels given in (c). The R-zeros cluster vertically above the resonance frequency and below the S-matrix zero frequency, as predicted by single resonance TCMT approximation Eq. (27). The common width of the constrictions for waveguides {4, 5, 6} is slightly tuned to make a three-in-three-out R-zero real, creating an RSM. (b) R-zero spectrum for the same junction but with the constrictions opened, which lowers the Q of the resonances (note change in vertical scale). The linewidths of the resonances are now comparable to their spacing. Due to multiresonance effects, the Rzeros are spread out along the real and complex frequency axis and are no longer associated with a single resonance. Nonetheless, by slightly tuning the constriction width as before, a three-in-three-out R-zero is again made real (RSM), as in the high-Q case. (c), (d) The mode profiles of the RSMs for the high-Q (c) and low-Q (d) cases.

will not be so in the sense defined by S, but rather by SS_0^{-1} , which in some cases will actually be a "transmissionless" mode of S.

F. R-zeros and RSMs as eigenmodes of the wave operator

We have introduced two equivalent equations to solve for R-zeros and RSMs: Eq. (2) in terms of a generalized reflection matrix, and Eq. (18) in terms of an effective wave operator. Both define nonlinear eigenproblems, and both are applicable to any open system and for each of the $2^N - 2$ choices of reflectionless input channels. While Eq. (18) has the caveat that it can sometimes also yield BICs [48] or one-sided reso-

(a) Incident field (monopole)



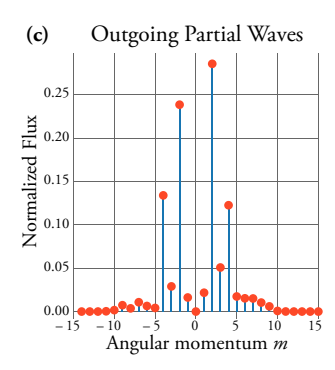


FIG. 6. Reflectionless scattering of a monopole scalar wave from a deformed disk dielectric resonator (n = 3) with mean radius \bar{R} , shown as shaded regions in (a) and (b). The disk boundary is $r(\theta)/\bar{R} = 1 + x\{0.8528\cos(2[\theta - 0.3127]) + 0.8346\cos(3[\theta - 0.0079])\}$, with x = 0.2768. The Monopolar RSM was achieved by tuning the single dimensionless parameter x until a given complex R-zero became real. The RSM frequency is at $\omega_0 \bar{R}/c = 6.4853$. (a) The input field only has an m = 0 component (pure monopole). (b) The outgoing field contains no m = 0 component, and is a coherent superposition of many other m's. (c) The outgoing flux, carried by each angular momentum channel m, normalized by the total incident flux. There is no outgoing flux for m = 0 because the structure was shape-tuned to a monopolar RSM. Note that since we have a purely real index here the RSM we have found must be bipolar, which implies that if we time reversed the complicated superposition of outgoing multipole radiation the incident wavefront would interfere perfectly to generate monopole-only outgoing radiation.

nances which are not reflectionless (see discussions at the end of Sec. II C), it is closer to the well-known resonance problem. In this section we discuss the details of solving for *R*-zeros through Eq. (18).

The distinguishing feature of the wave operator \hat{A}_{RZ} , as defined in Eq. (17), is the specific frequency-dependent self-energy, formally defined by Eq. (15), that acts on the surface and imposes the boundary condition as outgoing for the channels in \bar{F} and incoming for the channels in F. Below we describe two implementations, one based on the PML approach and one based on an extension of the "boundary-matching" conditions associated with purely outgoing or incoming waves [50,117]. We note that we regard the boundary-matching approach as more fundamental because it can be used to solve any R-zero problem, including those for which the asymptotic channels are not spatially separated (as in Fig. 6), whereas the PML method cannot. Moreover the PML method cannot easily handle problems where dielectric dispersion is important.

1. PML-based implementation of boundary conditions

The PML method, when applicable, typically will allow easier solution for the R-zeros, as the frequency dependence drops out of the boundary conditions, mapping the calculation to a linear eigenvalue problem which is readily solved by standard diagonalization (full or partial). This mapping is achieved by using impedance-matched absorbing layers called Perfectly Matched Layers [46,47], which create an effective outgoing boundary through an eigenvalue-independent modification of the bulk wave operator. Note that here we are not referring to the impedance matching of input waves which occurs at an R-zero, but the suppression of the reflection from the fictitious boundary layers which allow one to find purely outgoing solutions without boundary matching. Since PMLs always work for purely outgoing boundary conditions (if dispersion can be neglected), the PML method is the most commonly used method for finding resonances, at least in

photonics [4]. A fully incoming boundary condition, relevant for S-matrix zeros and CPA, while less common, can be similarly implemented with a PML through complex conjugation.

A left-to-right R-zero is an eigenmode of the wave operator with a conjugated PML on the left and a conventional PML on the right (and vice versa for a right-to-left *R*-zero); this type of solution has been demonstrated in the context of acoustic waveguides in Ref. [48]. The generalization of this to higher dimensions and a greater number of channels is straightforward: simply use an appropriate PML or conjugate PML for the propagating dimension in each of the asymptotic regions. This approach has been used for all of the examples in this paper except for the free-space example given below in Fig. 6, where the method would fail. The RSM problem for a six waveguide system coupled into a two-dimensional (2D) chaotic cavity shown in Fig. 5 is an example of a more complex geometry for which R-zeros and RSMs can be found using the PML method. Note that PMLs, both conventional and conjugated, must be used with caution, as they introduce additional "PML modes" in the eigenvalue spectrum, which need to be identified and discarded [4].

2. Mode-matching implementation of boundary conditions

For cases in which the asymptotic input channels are not spatially disjoint from the asymptotic output channels (as well as for all the cases where they are distinct), we can explicitly match the continuity conditions channel by channel, assigning the appropriate incoming or outgoing condition for that geometry. The general matching equation for a scalar field $\psi(\mathbf{x})$ is

$$\psi(\mathbf{x})|_{\partial\Omega} = \oint_{\partial\Omega} \left[G_F^{A,N}(\mathbf{x}, \mathbf{x}') + G_{\bar{F}}^{R,N}(\mathbf{x}, \mathbf{x}') \right] \nabla \psi(\mathbf{x}') \cdot d\mathbf{S}',$$
(28)

where $G_F^{A,N}$ is the advanced Green's function subject to a Neumann condition at the interface with the scattering region, restricted to the input channels F, and $G_{\bar{F}}^{R,N}$ is the retarded Green's function restricted to the output channels.

The surface integral is over $\partial\Omega$, which separates the scattering region Ω from the asymptotic regions $\bar{\Omega}$. We give the explicit, frequency-dependent boundary conditions for three geometries (1D systems, 2D strip multimode waveguides, and finite scatters in 2D free space) in Appendix B.

In Fig. 6, we provide an example for which the modematching approach must be used: a 2D deformed dielectric resonator in free space, which has been shape-tuned to have an RSM for monopole input at a given complex frequency, ω_0 . The theory here implies that one can perfectly impedance match a specific superposition of any number of coherent input multipoles to the remaining multipoles. Thus the scatterer when tuned to the RSM acts as a perfectly multipoletransforming antenna. In the example shown in Fig. 6, by tuning a single deformation parameter, we were able to find a *real* frequency at which the monopole input was reflectionless, so that all of the scattered waves were in higher multipoles. The R-zero nonlinear eigenvalue problem here was solved using NEP-PACK [118,119]. Through further optimization of the shape one presumably could enhance the scattered output into certain desired outgoing channels. Note that the scattering here is not perturbative and the output is not simply determined by single scattering from a particular multipole of the deformation.

The parameter x used to tune to an RSM is the overall strength of deformation, such that x = 0 yields a circular disk with no deformation. In the limit that $x \to 0$, continuous rotational symmetry is restored, the angular momentum scattering channels labeled by m decouple from each other, and the scattering matrix is diagonal. Therefore for x = 0, the R-zero frequencies are also S-matrix zeros, which are constrained by flux conservation to be in the upper half-plane. On the other hand, as the deformation x is made larger, the m channels become increasingly mixed, so that the single monopole input becomes coupled to more and more multipole outputs. The effective radiative loss will eventually overtake the effective radiative gain and push the *R*-zeros into the lower half-plane. Therefore by continuity there will be a deformation strength x_0 at which the R-zero crosses the real axis, becoming an RSM.

III. SUMMARY AND CONCLUSIONS

This paper presents a general theory of impedance matching of waves to finite structures of arbitrary geometry in any dimension, focusing on the case of electromagnetics waves and assuming short-ranged scattering interactions. The theory is expressed in terms of tuning complex frequency reflectionless solutions of the wave equation to the real axis to become physical steady-state solutions that are perfectly impedance matched at the input frequency. A generalized reflection matrix is defined which describes a chosen set of input channels, and its zero eigenvalues and eigenvectors give the frequencies and wavefronts which will lead to zero reflection back into those channels, with scattering into the complementary channels as well as possible absorption or amplification in the structure, depending on the presence of active media within the scattering region. When these solutions are tuned to real

frequency we refer to them as reflectionless scattering modes. When the correct RSM wavefront is imposed on the structure, the total reflection into the chosen channels will exhibit a quadratic dip to zero with the same linewidth as the usual resonances (at the same tuning parameters). The framework given here applies to all linear classical wave scattering, and to quantum scattering as well, as long as the scattering potential is short-ranged. Without special symmetries RSMs will not exist for an arbitrary structure and tuning either by changing geometric parameters of the cavity or scatterer or by adding loss or gain is necessary to create them. In the case of \mathcal{P} - and \mathcal{T} -symmetric (lossless) scatterers, RSMs do appear as the bidirectional unit transmission resonances familiar from elementary textbook examples, and the same is true for PT-symmetric scatterers, but in the latter case they are unidirectional. In both cases the RSMs can disappear without breaking the symmetry of the structure above a spontaneous PT-symmetry-breaking transition that occurs at an EP. These represent a different type of EP in terms of their physical manifestation, and unlike the widely studied resonant EPs they can occur on the real axis without generating a self-oscillation instability.

Our results can be most naturally applied to classical electromagnetic scattering and acoustic scattering. Our paper shows that by varying a single continuous tuning parameter the impedance-matched states corresponding to the RSM boundary conditions can be created. However it must be noted that impedance matching is only possible for structures with many radiative channels by exciting the structure with the appropriate coherent wavefront, which requires full phase and amplitude control of the illuminating source. Moreover, other desirable states cannot be engineered by tuning a single parameter; e.g., similar to Ref. [120], in a three-mode waveguide junction a state with input in waveguide 1, which is both reflectionless and only scatters into waveguide 2, and not into waveguide 3, does not correspond to the RSM boundary condition. Our theory shows that this cannot be achieved with single parameter tuning and suggests that it is not guaranteed to exist if more parameters are tuned. Nonetheless, if such a state is desired one could search for it by first finding the RSM with one channel in and two out, and then optimizing further parameters so as to minimize the scattering into waveguide 3. There are indications in our current results that such an optimization could be successful and may provide a powerful tool for design in photonics and acoustics.

Since the theory of RSMs can determine a perfectly impedance-matched steady state of linear Maxwell electrodynamics, it will also determine an impedance-matched state for quantum electrodynamics, for which all moments of the reflected flux will vanish at ω_{RZ} . Quantum fluctuations will arise only due to the finite linewidth of the input field [121]. Therefore the RSM concept can be of interest in quantum optics too.

ACKNOWLEDGMENTS

W.R.S. and A.D.S. acknowledge the support of the NSF Condensed Matter and Materials Theory (CMMT) program under Grant No. DMR-1743235.

APPENDIX A: DERIVATION OF DETERMINANT RELATIONS

In this Appendix we derive (10) for an N-channel S matrix, and (16) for an N_{in} -input generalized reflection matrix \mathbf{R}_{in} , using the two identities

$$(\mathbf{A} + \mathbf{BC})^{-1}\mathbf{B} = \mathbf{A}^{-1}\mathbf{B}(\mathbf{I}_M + \mathbf{C}\mathbf{A}^{-1}\mathbf{B})^{-1}, \quad (A1)$$

$$\det(\mathbf{I}_N - \mathbf{BC}) = \det(\mathbf{I}_M - \mathbf{CB}), \tag{A2}$$

for invertible $\mathbf{A} \in \mathbb{C}^{N \times N}$, and arbitrary $\mathbf{B} \in \mathbb{C}^{N \times M}$, $\mathbf{C} \in \mathbb{C}^{M \times N}$, which we now derive.

The first identity is a generalization of the "push-through identity" [76]

$$(\mathbf{I}_N + \mathbf{B}\mathbf{D})^{-1}\mathbf{B} = \mathbf{B}(\mathbf{I}_M + \mathbf{D}\mathbf{B})^{-1}, \tag{A3}$$

with $\mathbf{D} \in \mathbb{C}^{M \times N}$, and \mathbf{B} as before. It is named for its action on \mathbf{B} relative to the inverse, and follows trivially from noting that $\mathbf{B}(\mathbf{I}_M + \mathbf{D}\mathbf{B}) = (\mathbf{I}_N + \mathbf{B}\mathbf{D})\mathbf{B}$. This can be generalized for $\mathbf{A}, \mathbf{B}, \mathbf{C}$, with $\mathbf{A} \in \mathbb{C}^{N \times N}$ invertible by starting with $(\mathbf{A} + \mathbf{B}\mathbf{C})^{-1} = \mathbf{A}^{-1}(\mathbf{I}_N + \mathbf{B}\mathbf{C}\mathbf{A}^{-1})^{-1}$. Applying Eq. (A3), with $\mathbf{D} = \mathbf{C}\mathbf{A}^{-1}$, we arrive at

$$(\mathbf{A} + \mathbf{BC})^{-1}\mathbf{B} = \mathbf{A}^{-1}\mathbf{B}(\mathbf{I}_M + \mathbf{C}\mathbf{A}^{-1}\mathbf{B})^{-1}, \quad (A4)$$

which proves the first identity.

The second identity can be derived as a special case of Schur's determinant formula [122]

$$\det \mathbf{A} \det(\mathbf{D} - \mathbf{C}\mathbf{A}^{-1}\mathbf{B}) = \det \mathbf{D} \det(\mathbf{A} - \mathbf{B}\mathbf{D}^{-1}\mathbf{C}) \quad (A5)$$

where **A**, **B**, **C** are defined as before, and $\mathbf{D} \in \mathbb{C}^{M \times M}$ is invertible. The judicious choice $\mathbf{A} = \mathbf{I}_N$, $\mathbf{D} = \mathbf{I}_M$ gives

$$\det(\mathbf{I}_N - \mathbf{BC}) = \det(\mathbf{I}_M - \mathbf{CB}), \tag{A6}$$

which is what we wanted to show.

1. Evaluating det $S(\omega)$

Applying Eq. (A1) to $(\mathbf{A}_0' - \mathbf{\Delta} + i\mathbf{\Gamma})^{-1}\mathbf{W}_p$, recalling that $\mathbf{\Gamma} = \pi \mathbf{W}_p \mathbf{W}_p^{\dagger}$, yields

$$(\mathbf{A}_0' - \mathbf{\Delta} + i\mathbf{\Gamma})^{-1}\mathbf{W}_p = \mathbf{G}_0''\mathbf{W}_p(\mathbf{I}_N + i\pi \mathbf{W}_p^{\dagger}\mathbf{G}_0''\mathbf{W}_p)^{-1},$$
(A7)

where $\mathbf{G}_0'' = (\mathbf{A}_0' - \mathbf{\Delta})^{-1}$. Using this in the full expression for the S matrix (8) and (9), and factoring out $(\mathbf{I}_N + i\pi \mathbf{W}_p^{\dagger} \mathbf{G}_0'' \mathbf{W}_p)^{-1}$,

$$\mathbf{S} = (\mathbf{I}_N - i\pi \mathbf{W}_p^{\dagger} \mathbf{G}_0^{\prime\prime} \mathbf{W}_p) / (\mathbf{I}_N + i\pi \mathbf{W}_p^{\dagger} \mathbf{G}_0^{\prime\prime} \mathbf{W}_p). \tag{A8}$$

Taking the determinant and applying Eq. (A2) to the numerator and denominator, we have

$$\det \mathbf{S} = \frac{\det(\mathbf{I} - i\pi \mathbf{G}_0'' \mathbf{W}_p \mathbf{W}_p^{\dagger})}{\det(\mathbf{I} + i\pi \mathbf{G}_0'' \mathbf{W}_p \mathbf{W}_p^{\dagger})} = \frac{\det(\mathbf{A}_0' - \mathbf{\Delta} - i\mathbf{\Gamma})}{\det(\mathbf{A}_0' - \mathbf{\Delta} + i\mathbf{\Gamma})}, \quad (A9)$$

where I is the identity on the (infinite-dimensional) closed-cavity Hilbert space. This proves Eq. (10).

2. Evaluating det $R_{in}(\omega)$

We proceed as we did with the S matrix, but starting with \mathbf{R}_{in} from (14), where F defines the inputs: push \mathbf{W}_F through

 $G_{\rm eff}$, factor out a common inverse, take the determinant, and apply (A2).

Writing G_{eff} in (14) in terms of W_F and $W_{\bar{F}}$, and using the identity (A1), yields

$$(\bar{\mathbf{A}}_0 + i\mathbf{\Gamma}_F)^{-1}\mathbf{W}_F = \bar{\mathbf{A}}_0^{-1}\mathbf{W}_F(\mathbf{I}_{N_{\text{in}}} + i\pi\mathbf{W}_F^{\dagger}\bar{\mathbf{A}}_0^{-1}\mathbf{W}_F)^{-1},$$
(A10)

where $\bar{\mathbf{A}}_0 \equiv \mathbf{A}_0' - \mathbf{\Delta} + i\mathbf{\Gamma}_{\bar{F}}$. See (9) and (15) for the definitions of $\mathbf{\Delta}$, $\mathbf{\Gamma}_{F,\bar{F}}$, and $\mathbf{W}_{F,\bar{F}}$.

Plugging this into (14) and factoring out $(\mathbf{I}_{N_{\text{in}}} + i\pi \mathbf{W}_F^{\dagger} \bar{\mathbf{A}}_0^{-1} \mathbf{W}_F)^{-1}$ gives a K-matrix representation for \mathbf{R}_{in} :

$$\mathbf{R}_{\text{in}} = \left(\mathbf{I}_{N_{\text{in}}} - i\pi \mathbf{W}_F^{\dagger} \bar{\mathbf{A}}_0^{-1} \mathbf{W}_F\right) / \left(\mathbf{I}_{N_{\text{in}}} + i\pi \mathbf{W}_F^{\dagger} \bar{\mathbf{A}}_0^{-1} \mathbf{W}_F\right). \tag{A11}$$

Taking the determinant, using the identity (A2), and multiplying the numerator and denominator by det \bar{A}_0 results in

$$\det \mathbf{R}_{\text{in}} = \frac{\det \left(\mathbf{I} - i\pi \bar{\mathbf{A}}_0^{-1} \mathbf{W}_F \mathbf{W}_F^{\dagger} \right)}{\det \left(\mathbf{I} + i\pi \bar{\mathbf{A}}_0^{-1} \mathbf{W}_F \mathbf{W}_F^{\dagger} \right)}$$
(A12)

$$= \frac{\det(\mathbf{A}' - \mathbf{\Delta} + i\mathbf{\Gamma}_{\bar{F}} - i\mathbf{\Gamma}_{F})}{\det(\mathbf{A}'_{0} - \mathbf{\Delta} + i\mathbf{\Gamma}_{\bar{F}} + i\mathbf{\Gamma}_{F})}.$$
 (A13)

Finally, using the identities for the filters **F** and $\bar{\mathbf{F}}$ (12), the denominator can be simplified by $\mathbf{\Gamma}_F + \mathbf{\Gamma}_{\bar{F}} = \mathbf{\Gamma}$. This proves Eq. (16).

APPENDIX B: EXPLICIT FORMS OF BOUNDARY MATCHING

(1) In one dimension, with the scattering region contained entirely in |x| < a, the RSM boundary conditions are

left-incident:
$$\psi(\pm a) = +\partial_x \psi(\pm a)/i(\omega/c)$$
, (B1)

right-incident:
$$\psi(\pm a) = -\partial_x \psi(\pm a)/i(\omega/c)$$
. (B2)

(2) For a metallic waveguide with transverse width t in two dimensions, and with the scattering region contained entirely in |x| < a, the RSM boundary conditions are

$$\psi(\pm a, y) = \mp \int dy' K_{F_{\pm}}(y, y') \, \partial_x \psi(\pm a, y')$$
 (B3)

where F_- is the set of input channels for the left lead, and F_+ for the right. The kernel K_F is

$$K_F(y, y') = \sum_{m \in F} g_m^-(y, y') + \sum_{m \notin F} g_m^+(y, y'),$$
 (B4)

where

$$g_m^{\pm}(y, y') = \pm \frac{1}{i\beta_m^{\pm}(\omega)} \sin\left(\frac{m\pi y}{t}\right) \sin\left(\frac{m\pi y'}{t}\right).$$
 (B5)

For real ω , the propagation constant is

$$\beta_m^{\pm}(\omega) = \sqrt{\left(\frac{\omega}{c}\right)^2 - \left(\frac{m\pi}{t}\right)^2 \pm i0^+}.$$
 (B6)

The square-root branch cut is the conventional one along the negative real axis, such that $\sqrt{-1 \pm i0^+} = \pm i$. It is worth noting that the contribution of each propagating mode to K_F has a sign which depends on whether the mode is designated as input or output, while the nonpropagating modes all contribute with the same sign, regardless of the choice of F. For complex

 ω , the construction of the propagation constant β_m is more involved, and beyond the scope of this paper [123].

(3) A finite scatterer in 2D free space, contained entirely within a radius R, has asymptotic channels specified by angular momentum m. The R-zero boundary condition is

$$\psi(R,\phi) = \int_0^{2\pi} d\phi' \sum_{m} \frac{e^{im(\phi-\phi')}}{2\pi c_m^F(kR)} \partial_r \psi(R,\phi'), \qquad (B7)$$

where

$$c_m^F(x) = \begin{cases} \partial_R \ln H_m^{(2)}(x), & m \in F \\ \partial_R \ln H_m^{(1)}(x), & m \notin F. \end{cases}$$
(B8)

- which is advanced in the input channels F and retarded in the (B7)output channels \bar{F} : $|\psi(\mathbf{x})|_{\partial\Omega} = \oint_{\partial\Omega} \left[G_F^{A,N}(\mathbf{x}, \mathbf{x}') + G_F^{R,N}(\mathbf{x}, \mathbf{x}') \right] \nabla \psi(\mathbf{x}') \cdot d\mathbf{S}'.$
 - The derivation of this takes us too far from the main thread of this paper, and will be discussed in a future publication.

 $H_m^{(1,2)}(x)$ are the Hankel functions of the first and second kind

[Eqs. (B1)–(B8)] are specific instances of a general formula

which relates the function at the boundary $\partial \Omega$ to its normal derivative via the appropriate Green's function, subject to a Neumann condition at the interface with the scattering region,

All of the boundary conditions delineated above

(outgoing and incoming, respectively) of order m [124].

- [1] G. Gamow, Zur quantentheorie des atomkernes, Z. Phys. 51, 204 (1928).
- [2] A. Böhm, Resonance poles and Gamow vectors in the rigged Hilbert space formulation of quantum mechanics, J. Math. Phys. 22, 2813 (1981).
- [3] E. S. C. Ching, P. T. Leung, A. M. van den Brink, W. M. Suen, S. S. Tong, and K. Young, Quasinormal-mode expansion for waves in open systems, Rev. Mod. Phys. 70, 1545 (1998).
- [4] P. Lalanne, W. Yan, K. Vynck, C. Sauvan, and J.-P. Hugonin, Light interaction with photonic and plasmonic resonances, Laser Photonics Rev. 12, 1700113 (2018).
- [5] R. Lang, M. O. Scully, and W. E. Lamb, Jr., Why is the laser line so narrow? A theory of single-quasimode laser operation, Phys. Rev. A 7, 1788 (1973).
- [6] L. Ge, Y. Chong, and A. D. Stone, Steady-state ab initio laser theory: Generalizations and analytic results, Phys. Rev. A 82, 063824 (2010).
- [7] S. Esterhazy, D. Liu, M. Liertzer, A. Cerjan, L. Ge, K. G. Makris, A. D. Stone, J. M. Melenk, S. G. Johnson, and S. Rotter, Scalable numerical approach for the steady-state ab initio laser theory, Phys. Rev. A 90, 023816 (2014).
- [8] Y. D. Chong, L. Ge, H. Cao, and A. D. Stone, Coherent Perfect Absorbers: Time-Reversed Lasers, Phys. Rev. Lett. 105,
- [9] W. Wan, Y. Chong, L. Ge, H. Noh, A. D. Stone, and H. Cao, Time-reversed lasing and interferometric control of absorption, Science 331, 889 (2011).
- [10] D. G. Baranov, A. Krasnok, T. Shegai, A. Alù, and Y. Chong, Coherent perfect absorbers: Linear control of light with light, Nat. Rev. Mater. 2, 17064 (2017).
- [11] K. Pichler, M. Kühmayer, J. Böhm, A. Brandstötter, P. Ambichl, U. Kuhl, and S. Rotter, Random anti-lasing through coherent perfect absorption in a disordered medium, Nature (London) 567, 351 (2019).
- [12] C. M. Bender and S. Boettcher, Real Spectra in Non-Hermitian Hamiltonians Having PT Symmetry, Phys. Rev. Lett. 80, 5243
- [13] A. Regensburger, C. Bersch, M.-A. Miri, G. Onishchukov, D. N. Christodoulides, and U. Peschel, Parity-time synthetic photonic lattices, Nature (London) 488, 167 (2012).

- [14] L. Feng, Z. J. Wong, R.-M. Ma, Y. Wang, and X. Zhang, Single-mode laser by parity-time symmetry breaking, Science **346**, 972 (2014).
- [15] H. Hodaei, M.-A. Miri, M. Heinrich, D. N. Christodoulides, and M. Khajavikhan, Parity-time-symmetric microring lasers, Science 346, 975 (2014).
- [16] B. Peng, Ş. K. Özdemir, F. Lei, F. Monifi, M. Gianfreda, G. L. Long, S. Fan, F. Nori, C. M. Bender, and L. Yang, Parity-time-symmetric whispering-gallery microcavities, Nat. Phys. 10, 394 (2014).
- [17] L. Feng, R. El-Ganainy, and L. Ge, Non-Hermitian photonics based on parity-time symmetry, Nat. Photonics 11, 752 (2017).
- [18] R. El-Ganainy, K. G. Makris, M. Khajavikhan, Z. H. Musslimani, S. Rotter, and D. N. Christodoulides, Non-Hermitian physics and PT symmetry, Nat. Phys. 14, 11 (2018).
- [19] Ş. K. Özdemir, S. Rotter, F. Nori, and L. Yang, Parity-time symmetry and exceptional points in photonics, Nat. Mater. 18, 783 (2019).
- [20] M.-A. Miri and A. Alù, Exceptional points in optics and photonics, Science 363, eaar7709 (2019).
- [21] Z. Lin, H. Ramezani, T. Eichelkraut, T. Kottos, H. Cao, and D. N. Christodoulides, Unidirectional Invisibility Induced by PT-Symmetric Periodic Structures, Phys. Rev. Lett. 106, 213901 (2011).
- [22] H. Hernandez-Coronado, D. Krejčiřík, and P. Siegl, Perfect transmission scattering as a PT-symmetric spectral problem, Phys. Lett. A 375, 2149 (2011).
- [23] S. Longhi, Invisibility in \mathcal{PT} -symmetric complex crystals, J. Phys. A: Math. Theor. 44, 485302 (2011).
- [24] L. Ge, Y. D. Chong, and A. D. Stone, Conservation relations and anisotropic transmission resonances in one-dimensional PT-symmetric photonic heterostructures, Phys. Rev. A 85, 023802 (2012).
- [25] H. F. Jones, Analytic results for a PT-symmetric optical structure, J. Phys. A 45, 135306 (2012).
- L. Feng, Y.-L. Xu, W. S. Fegadolli, M.-H. Lu, J. E. B. Oliveira, V. R. Almeida, Y.-F. Chen, and A. Scherer, Experimental demonstration of a unidirectional reflectionless parity-time metamaterial at optical frequencies, Nat. Mater. **12**, 108 (2013).

- [27] H. Ramezani, H.-K. Li, Y. Wang, and X. Zhang, Unidirectional Spectral Singularities, Phys. Rev. Lett. 113, 263905 (2014).
- [28] B. Midya, Supersymmetry-generated one-way-invisible $\mathcal{P}T$ -symmetric optical crystals, Phys. Rev. A **89**, 032116 (2014).
- [29] R. Fleury, D. Sounas, and A. Alù, An invisible acoustic sensor based on parity-time symmetry, Nat. Commun. 6, 5905 (2015).
- [30] Nicolas X. A. Rivolta and B. Maes, Side-coupled resonators with parity-time symmetry for broadband unidirectional invisibility, Phys. Rev. A 94, 053854 (2016).
- [31] L. Jin, X. Z. Zhang, G. Zhang, and Z. Song, Reciprocal and unidirectional scattering of parity-time symmetric structures, Sci. Rep. 6, 20976 (2016).
- [32] Y. Fu, Y. Xu, and H. Chen, Zero index metamaterials with PT symmetry in a waveguide system, Opt. Express 24, 1648 (2016).
- [33] E. Yang, Y. Lu, Y. Wang, Y. Dai, and P. Wang, Unidirectional reflectionless phenomenon in periodic ternary layered material, Opt. Express 24, 14311 (2016).
- [34] M. Sarısaman, Unidirectional reflectionlessness and invisibility in the TE and TM modes of a PT-symmetric slab system, Phys. Rev. A 95, 013806 (2017).
- [35] M. Sarısaman and M. Tas, Unidirectional invisibility and \mathcal{PT} symmetry with graphene, Phys. Rev. B **97**, 045409 (2018).
- [36] Y. Huang, Y. Shen, C. Min, S. Fan, and G. Veronis, Unidirectional reflectionless light propagation at exceptional points, Nanophotonics **6**, 977 (2017).
- [37] A. Mostafazadeh, Invisibility and PT symmetry, Phys. Rev. A 87, 012103 (2013).
- [38] G. Castaldi, S. Savoia, V. Galdi, A. Alù, and N. Engheta, PT Metamaterials via Complex-Coordinate Transformation Optics, Phys. Rev. Lett. 110, 173901 (2013).
- [39] Y. Shen, X. H. Deng, and L. Chen, Unidirectional invisibility in a two-layer non-PT-symmetric slab, Opt. Express 22, 19440 (2014).
- [40] J.-H. Wu, M. Artoni, and G. C. La Rocca, Non-Hermitian Degeneracies and Unidirectional Reflectionless Atomic Lattices, Phys. Rev. Lett. **113**, 123004 (2014).
- [41] S. A. R. Horsley, M. Artoni, and G. C. La Rocca, Spatial Kramers-Kronig relations and the reflection of waves, Nat. Photonics 9, 436 (2015).
- [42] J.-H. Wu, M. Artoni, and G. C. La Rocca, Parity-time-antisymmetric atomic lattices without gain, Phys. Rev. A **91**, 033811 (2015).
- [43] J. Gear, Y. Sun, S. Xiao, L. Zhang, R. Fitzgerald, S. Rotter, H. Chen, and J. Li, Unidirectional zero reflection as gauged parity-time symmetry, New J. Phys. 19, 123041 (2017).
- [44] K. G. Makris, A. Brandstötter, P. Ambichl, Z. H. Musslimani, and S. Rotter, Wave propagation through disordered media without backscattering and intensity variations, Light: Sci. Appl. 6, e17035 (2017).
- [45] A. Brandstötter, K. G. Makris, and S. Rotter, Scattering-free pulse propagation through invisible non-Hermitian media, Phys. Rev. B **99**, 115402 (2019).
- [46] J.-P. Berenger, A perfectly matched layer for the absorption of electromagnetic waves, J. Comput. Phys. **114**, 185 (1994).
- [47] A. Oskooi and S. G. Johnson, in *Advances in FDTD Computational Electrodynamics*, edited by A. Taflove, A. Oskooi, and S. G. Johnson (Artech House, Boston, 2013), Chap. 5.

- [48] A.-S. Bonnet-Ben Dhia, L. Chesnel, and V. Pagneux, Trapped modes and reflectionless modes as eigenfunctions of the same spectral problem, Proc. R. Soc. A 474, 20180050 (2018).
- [49] C. W. Hsu, B. Zhen, A. D. Stone, J. D. Joannopoulos, and M. Soljačić, Bound states in the continuum, Nat. Rev. Mater. 1, 16048 (2016).
- [50] H. E. Türeci, Harald G. L. Schwefel, Ph. Jacquod, and A. D. Stone, in *Progress in Optics*, edited by E. Wolf (Elsevier, Amsterdam, 2005), Vol. 47, Chap. 2, pp. 75–135.
- [51] H. A. Haus, *Waves and Fields in Optoelectronics* (Prentice-Hall, Englewood Cliffs, NJ, 1984), Chap. 7.
- [52] A. Yariv, Universal relations for coupling of optical power between microresonators and dielectric waveguides, Electron. Lett. 36, 321 (2000).
- [53] M. Cai, O. Painter, and K. J. Vahala, Observation of Critical Coupling in a Fiber Taper to a Silica-Microsphere Whispering-Gallery Mode System, Phys. Rev. Lett. 85, 74 (2000).
- [54] D. Jalas, A. Petrov, M. Eich, W. Freude, S. Fan, Z. Yu, R. Baets, M. Popović, A. Melloni, J. D. Joannopoulos, M. Vanwolleghem, C. R. Doerr, and H. Renner, What is—and what is not—an optical isolator, Nat. Photonics 7, 579 (2013).
- [55] G. H. Golub and H. A. van der Vorst, Eigenvalue computation in the 20th century, J. Comput. Appl. Math. 123, 35 (2000).
- [56] A. Friedman and M. Shinbrot, Nonlinear eigenvalue problems, Acta Math. 121, 77 (1968).
- [57] J. Asakura, T. Sakurai, H. Tadano, I. Tsutomu, and K. Kimura, A numerical method for polynomial eigenvalue problems using contour integral, Jpn. J. Ind. Appl. Math. 27, 73 (2010).
- [58] Y. Su and Z. Bai, Solving rational eigenvalue problems via linearization, SIAM J. Matrix Anal. Appl. 32, 201 (2011).
- [59] Wolf-Jürgen Beyn, An integral method for solving nonlinear eigenvalue problems, Linear Algebra Appl. 436, 3839 (2012).
- [60] N. D. Mermin, The topological theory of defects in ordered media, Rev. Mod. Phys. 51, 591 (1979).
- [61] B. Zhen, C. W. Hsu, L. Lu, A. D. Stone, and M. Soljačić, Topological Nature of Optical Bound States in the Continuum, Phys. Rev. Lett. 113, 257401 (2014).
- [62] Y. Guo, M. Xiao, and S. Fan, Topologically Protected Complete Polarization Conversion, Phys. Rev. Lett. 119, 167401 (2017).
- [63] M. Reed and B. Simon, *Methods of Modern Mathematical Physics III: Scattering Theory* (Academic, London, 1979).
- [64] C. Mahaux and H. A. Weidenmüller, Shell-Model Approach to Nuclear Reactions (North-Holland, Amsterdam, 1969).
- [65] C. W. J. Beenakker, Random-matrix theory of quantum transport, Rev. Mod. Phys. 69, 731 (1997).
- [66] C. Viviescas and G. Hackenbroich, Field quantization for open optical cavities, Phys. Rev. A 67, 013805 (2003).
- [67] S. Rotter and S. Gigan, Light fields in complex media: Mesoscopic scattering meets wave control, Rev. Mod. Phys. 89, 015005 (2017).
- [68] C. Bloch, Une formulation unifiée de la théorie des réactions nucléaires, Nucl. Phys. 4, 503 (1957).
- [69] H. Feshbach, The optical model and its justification, Annu. Rev. Nucl. Sci. **8**, 49 (1958).
- [70] H. Feshbach, Unified theory of nuclear reactions, Ann. Phys. (NY) 5, 357 (1958).
- [71] U. Fano, Effects of configuration interaction on intensities and phase shifts, Phys. Rev. 124, 1866 (1961).

- [72] A. M. Lane and D. Robson, Comprehensive formalism for nuclear reaction problems. I. Derivation of existing reaction theories, Phys. Rev. **151**, 774 (1966).
- [73] H. Nishioka and H. A. Weidenmüller, Compound-nucleus scattering in the presence of direct reactions, Phys. Lett. B 157, 101 (1985).
- [74] F.-M. Dittes, The decay of quantum systems with a small number of open channels, Phys. Rep. **339**, 215 (2000).
- [75] A. F. Sadreev and I. Rotter, S-matrix theory for transmission through billiards in tight-binding approach, J. Phys. A: Math. Gen. 36, 11413 (2003).
- [76] D. S. Bernstein, Scalar, Vector, and Matrix Mathematics (Princeton University, Princeton, NJ, 2018).
- [77] W. MacDonald and A. Mekjian, Fine structure in nuclear resonances, Phys. Rev. 160, 730 (1967).
- [78] R. G. Newton, in *Scattering Theory of Waves and Particles*, 2nd ed., edited by W. Beiglböck, E. H Lieb, and W. Thirring (Springer, New York, 1982), Chap. 7.
- [79] V. Grigoriev, A. Tahri, S. Varault, B. Rolly, B. Stout, J. Wenger, and N. Bonod, Optimization of resonant effects in nanostructures via Weierstrass factorization, Phys. Rev. A 88, 011803(R) (2013).
- [80] A. Krasnok and A. Alù, Coherent control of light scattering, arXiv:1904.11384.
- [81] H. Zhou, B. Zhen, C. W. Hsu, O. D. Miller, S. G. Johnson, J. D. Joannopoulos, and M. Soljačić, Perfect single-sided radiation and absorption without mirrors, Optica 3, 1079 (2016).
- [82] X. Yin, J. Jin, M. Soljačić, C. Peng, and B. Zhen, Observation of topologically enabled unidirectional guided resonances, Nature (London) 580, 467 (2020).
- [83] A. E. Siegman, *Lasers* (University Science, Sausalito CA, 1986), Chap. 11.
- [84] L. Ge and H. E. Türeci, Antisymmetric \mathcal{PT} -photonic structures with balanced positive- and negative-index materials, Phys. Rev. A **88**, 053810 (2013).
- [85] Y. D. Chong, L. Ge, and A. D. Stone, PT-Symmetry Breaking and Laser-Absorber Modes in Optical Scattering Systems, Phys. Rev. Lett. 106, 093902 (2011).
- [86] T. Kato, *Perturbation Theory for Linear Operators* (Springer-Verlag, Berlin, 1995).
- [87] W. D. Heiss, The physics of exceptional points, J. Phys. A 45, 444016 (2012).
- [88] E. Persson, I. Rotter, H. J. Stöckmann, and M. Barth, Observation of Resonance Trapping in an Open Microwave Cavity, Phys. Rev. Lett. 85, 2478 (2000).
- [89] I. Rotter, A non-Hermitian Hamilton operator and the physics of open quantum systems, J. Phys. A: Math. Theor. **42**, 153001 (2009).
- [90] M. Liertzer, L. Ge, A. Cerjan, A. D. Stone, H. E. Türeci, and S. Rotter, Pump-Induced Exceptional Points in Lasers, Phys. Rev. Lett. 108, 173901 (2012).
- [91] M. Brandstetter, M. Liertzer, C. Deutsch, P. Klang, J. Schöberl, H. E. Türeci, G. Strasser, K. Unterrainer, and S. Rotter, Reversing the pump dependence of a laser at an exceptional point, Nat. Commun. 5, 4034 (2014).
- [92] J. Wiersig, Enhancing the Sensitivity of Frequency and Energy Splitting Detection by Using Exceptional Points: Application to Microcavity Sensors for Single-Particle Detection, Phys. Rev. Lett. 112, 203901 (2014).

- [93] B. Zhen, C. W. Hsu, Y. Igarashi, L. Lu, I. Kaminer, A. Pick, S.-L. Chua, J. D. Joannopoulos, and M. Soljačić, Spawning rings of exceptional points out of Dirac cones, Nature (London) 525, 354 (2015).
- [94] B. Peng, Ş. K. Özdemir, M. Liertzer, W. Chen, J. Kramer, H. Yılmaz, J. Wiersig, S. Rotter, and L. Yang, Chiral modes and directional lasing at exceptional points, Proc. Natl. Acad. Sci. USA 113, 6845 (2016).
- [95] W. Chen, Ş. K. Özdemir, G. Zhao, J. Wiersig, and L. Yang, Exceptional points enhance sensing in an optical microcavity, Nature (London) 548, 192 (2017).
- [96] H. Hodaei, A. U. Hassan, S. Wittek, H. Garcia-Gracia, R. El-Ganainy, D. N. Christodoulides, and M. Khajavikhan, Enhanced sensitivity at higher-order exceptional points, Nature (London) 548, 187 (2017).
- [97] H. Zhou, C. Peng, Y. Yoon, C. W. Hsu, K. A. Nelson, L. Fu, J. D. Joannopoulos, M. Soljačić, and B. Zhen, Observation of bulk Fermi arc and polarization half charge from paired exceptional points, Science 359, 1009 (2018).
- [98] M. Zhang, W. Sweeney, C. W. Hsu, L. Yang, A. D. Stone, and L. Jiang, Quantum Noise Theory of Exceptional Point Amplifying Sensors, Phys. Rev. Lett. 123, 180501 (2019).
- [99] V. Achilleos, G. Theocharis, O. Richoux, and V. Pagneux, Non-Hermitian acoustic metamaterials: Role of exceptional points in sound absorption, Phys. Rev. B 95, 144303 (2017).
- [100] W. R. Sweeney, C. W. Hsu, S. Rotter, and A. D. Stone, Perfectly Absorbing Exceptional Points and Chiral Absorbers, Phys. Rev. Lett. 122, 093901 (2019).
- [101] F. Cannata, J.-P. Dedonder, and A. Ventura, Scattering in PT-symmetric quantum mechanics, Ann. Phys. (NY) 322, 397 (2007).
- [102] L. Feng, X. Zhu, S. Yang, H. Zhu, P. Zhang, X. Yin, Y. Wang, and X. Zhang, Demonstration of a large-scale optical exceptional point structure, Opt. Express 22, 1760 (2014).
- [103] M. Kang, H.-X. Cui, T.-F. Li, J. Chen, W. Zhu, and M. Premaratne, Unidirectional phase singularity in ultrathin metamaterials at exceptional points, Phys. Rev. A 89, 065801 (2014).
- [104] K. Wisal, W. R. Sweeney, C. H. Hsu, and A. D. Stone, Manuscript in preparation.
- [105] A. A. Gorbatsevich and N. M. Shubin, Phys. Rev. B 96, 205441 (2017).
- [106] S. Fan, W. Suh, and J. D. Joannopoulos, Temporal coupled-mode theory for the Fano resonance in optical resonators, J. Opt. Soc. Am. A 20, 569 (2003).
- [107] W. Suh, Z. Wang, and S. Fan, Temporal coupled-mode theory and the presence of non-orthogonal modes in lossless multimode cavities, IEEE J. Quantum Electron. 40, 1511 (2004).
- [108] K. X. Wang, Time-reversal symmetry in temporal coupled-mode theory and nonreciprocal device applications, Opt. Lett. 43, 5623 (2018).
- [109] Z. Zhao, C. Guo, and S. Fan, Connection of temporal coupled-mode-theory formalisms for a resonant optical system and its time-reversal conjugate, Phys. Rev. A 99, 033839 (2019).
- [110] F. Alpeggiani, N. Parappurath, E. Verhagen, and L. Kuipers, Quasinormal-Mode Expansion of the Scattering Matrix, Phys. Rev. X 7, 021035 (2017).

- [111] L. Verslegers, Z. Yu, Z. Ruan, P. B. Catrysse, and S. Fan, From Electromagnetically Induced Transparency to Superscattering with a Single Structure: A Coupled-Mode Theory for Doubly Resonant Structures, Phys. Rev. Lett. 108, 083902 (2012).
- [112] C. W. Hsu, B. G. DeLacy, S. G. Johnson, J. D. Joannopoulos, and M. Soljačić, Theoretical criteria for scattering dark states in nanostructured particles, Nano Lett. 14, 2783 (2014).
- [113] C. Gardiner and P. Zoller, *Quantum Noise: A Handbook of Markovian and Non-Markovian Quantum Stochastic Methods with Applications to Quantum Optics*, 3rd ed. (Springer-Verlag, Berlin, 2004).
- [114] M. A. Woodbury, *Inverting Modified Matrices*, Memoranda Report No. 42 (Statistical Research Group, Princeton, NJ, 1950).
- [115] S. Fan, S. G. Johnson, J. D. Joannopoulos, C. Manolatou, and H. A. Haus, Waveguide branches in photonic crystals, J. Opt. Soc. Am. B 18, 162 (2001).
- [116] K. X. Wang, Z. Yu, S. Sandhu, V. Liu, and S. Fan, Condition for perfect antireflection by optical resonance at material interface, Optica 1, 388 (2014).
- [117] P. Ambichl, K. G. Makris, L. Ge, Y. Chong, A. D. Stone, and S. Rotter, Breaking of $\mathcal{P}T$ Symmetry in Bounded and Unbounded Scattering Systems, Phys. Rev. X 3, 041030 (2013).

- [118] J. Bezanson, A. Edelman, S. Karpinski, and V. B. Shah, Julia: A fresh approach to numerical computing, SIAM Review **59**, 65 (2017).
- [119] E. Jarlebring, M. Bennedich, G. Mele, E. Ringh, and P. Upadhyaya, NEP-PACK: A Julia package for nonlinear eigenproblems, arXiv:1811.09592.
- [120] L. Su, A. Y. Piggott, N. V. Sapra, J. Petykiewicz, and J. Vučković, Inverse design and demonstration of a compact on-chip narrowband three-channel wavelength demultiplexer, ACS Photonics 5, 301 (2017).
- [121] Y. D. Chong, H. Cao, and A. D. Stone, Noise properties of coherent perfect absorbers and critically coupled resonators, Phys. Rev. A 87, 013843 (2013).
- [122] *Handbook of Linear Algebra*, 2nd ed., edited by L. Hogben (CRC, Boca Raton, FL, 2013).
- [123] The propagation constant $\beta_m(\omega)$ for each mode has a sign ambiguity. One may try to resolve it for propagating modes by considering which sign corresponds to the correct sign of Re{ β_m }, as determined by F, and for evanescent modes by which one gives exponential decay far from the scattering region. However, the distinction between propagating and evanescent modes is itself ambiguous for complex ω , and must be determined by the asymptotic behavior of each mode when continued to the real axis.
- [124] M. Abramowitz and I. A. Stegun, Handbook of Mathematical Functions (Dover, New York, 1972).